

EUROPEAN ORGANISATION FOR NUCLEAR RESEARCH (CERN)



November 12, 2024

---

# Report from the NA61/SHINE experiment at the CERN SPS

The NA61/SHINE Collaboration

This document reports on the status and plans of the NA61/SHINE experiment at the CERN SPS as of November 2024. The document refers to the proposal SPSC-P-330

CERN-SPSC-2024-030 / SPSC-SR-353  
12/11/2024



# Contents

<b>1</b>	<b>Introduction</b>	<b>5</b>
<b>2</b>	<b>Data-taking summary</b>	<b>5</b>
2.1	Neutrino-related physics run, summer 2024 . . . . .	5
2.2	Strong interactions physics runs, autumn 2024 . . . . .	5
<b>3</b>	<b>Facility status</b>	<b>6</b>
3.1	Prototype DUNE long target . . . . .	7
3.2	Long Target Tracker . . . . .	7
<b>4</b>	<b>Software and calibration status</b>	<b>9</b>
4.1	Software . . . . .	9
4.2	Calibration . . . . .	10
<b>5</b>	<b>New results</b>	<b>12</b>
5.1	New results for strong interaction physics . . . . .	12
5.2	New results for neutrino physics . . . . .	26
5.3	New results for cosmic-ray physics . . . . .	29
<b>6</b>	<b>Beam request for 2025 and 2026 and plans after LS3</b>	<b>33</b>
6.1	Ion beams in 2025 and 2026 . . . . .	35
6.2	Hadron beams in 2025 and 2026 . . . . .	35
6.3	Plans after LS3 . . . . .	35
<b>7</b>	<b>Summary</b>	<b>36</b>

## The NA61/SHINE Collaboration

H. Adhikary <sup>11</sup>, P. Adrich <sup>13</sup>, K.K. Allison <sup>24</sup>, N. Amin <sup>4</sup>, E.V. Andronov <sup>20</sup>, I.-C. Arsene <sup>10</sup>, M. Bajda <sup>14</sup>, Y. Balkova <sup>16</sup>, D. Battaglia <sup>23</sup>, A. Bazgir <sup>11</sup>, S. Bhosale <sup>12</sup>, M. Bielewicz <sup>13</sup>, A. Blondel <sup>3</sup>, M. Bogomilov <sup>2</sup>, Y. Bondar <sup>11</sup>, W. Bryliński <sup>19</sup>, J. Brzychczyk <sup>14</sup>, M. Buryakov <sup>20</sup>, A.F. Camino <sup>26</sup>, Y.D. Chandak <sup>24</sup>, M. Čirković <sup>21</sup>, M. Csanád <sup>6</sup>, J. Cybowska <sup>19</sup>, T. Czopowicz <sup>11</sup>, C. Dalmazzone <sup>3</sup>, N. Davis <sup>12</sup>, A. Dmitriev <sup>20</sup>, P. von Doetinchem <sup>25</sup>, W. Dominik <sup>17</sup>, J. Dumarchez <sup>3</sup>, R. Engel <sup>4</sup>, G.A. Feofilov <sup>20</sup>, L. Fields <sup>23</sup>, Z. Fodor <sup>5,18</sup>, M. Friend <sup>7</sup>, M. Gaździcki <sup>11</sup>, K.E. Gollwitzer <sup>22</sup>, O. Golosov <sup>20</sup>, V. Golovatyuk <sup>20</sup>, M. Golubeva <sup>20</sup>, K. Grebieszko <sup>19</sup>, F. Guber <sup>20</sup>, P.G. Hurh <sup>22</sup>, S. Ilieva <sup>2</sup>, A. Ivashkin <sup>20</sup>, A. Izvestnyy <sup>20</sup>, N. Karpushkin <sup>20</sup>, M. Kiełbowicz <sup>12</sup>, V.A. Kireyeu <sup>20</sup>, R. Kolesnikov <sup>20</sup>, D. Kolev <sup>2</sup>, Y. Koshio <sup>8</sup>, S. Kowalski <sup>16</sup>, B. Kozłowski <sup>19</sup>, A. Krasnoperov <sup>20</sup>, W. Kucewicz <sup>15</sup>, M. Kuchowicz <sup>18</sup>, M. Kuich <sup>17</sup>, A. Kurepin <sup>20</sup>, A. László <sup>5</sup>, M. Lewicki <sup>12</sup>, G. Lykasov <sup>20</sup>, V.V. Lyubushkin <sup>20</sup>, M. Maćkowiak-Pawłowska <sup>19</sup>, A. Makhnev <sup>20</sup>, B. Maksiak <sup>13</sup>, A.I. Malakhov <sup>20</sup>, A. Marcinek <sup>12</sup>, A.D. Marino <sup>24</sup>, H.-J. Mathes <sup>4</sup>, T. Matulewicz <sup>17</sup>, V. Matveev <sup>20</sup>, G.L. Melkumov <sup>20</sup>, A. Merzlaya <sup>10</sup>, Ł. Mik <sup>15</sup>, S. Morozov <sup>20</sup>, Y. Nagai <sup>6</sup>, T. Nakadaira <sup>7</sup>, M. Naskręt <sup>18</sup>, S. Nishimori <sup>7</sup>, A. Olivier <sup>23</sup>, V. Ozvenchuk <sup>12</sup>, O. Panova <sup>11</sup>, V. Paolone <sup>26</sup>, O. Petukhov <sup>20</sup>, I. Pidhurskyi <sup>11</sup>, R. Płaneta <sup>14</sup>, P. Podlaski <sup>17</sup>, B.A. Popov <sup>20,3</sup>, B. Pórfy <sup>5,6</sup>, D.S. Prokhorova <sup>20</sup>, D. Pszczel <sup>13</sup>, S. Puławski <sup>16</sup>, R. Renfordt <sup>16</sup>, L. Ren <sup>24</sup>, V.Z. Reyna Ortiz <sup>11</sup>, D. Röhrich <sup>9</sup>, M. Roth <sup>4</sup>, Ł. Rozpłochowski <sup>12</sup>, M. Rummyantsev <sup>20</sup>, A. Rustamov <sup>1</sup>, M. Rybczynski <sup>11</sup>, A. Rybicki <sup>12</sup>, D. Rybka <sup>13</sup>, K. Sakashita <sup>7</sup>, K. Schmidt <sup>16</sup>, A. Seryakov <sup>20</sup>, P. Seyboth <sup>11</sup>, U.A. Shah <sup>11</sup>, Y. Shiraishi <sup>8</sup>, A. Shukla <sup>25</sup>, M. Słodkowski <sup>19</sup>, P. Staszal <sup>14</sup>, G. Stefanek <sup>11</sup>, J. Stepaniak <sup>13</sup>, Ł. Świdorski <sup>13</sup>, J. Szewiński <sup>13</sup>, R. Szukiewicz <sup>18</sup>, A. Taranenko <sup>20</sup>, A. Tefelska <sup>19</sup>, D. Tefelski <sup>19</sup>, V. Tereshchenko <sup>20</sup>, R. Tsenov <sup>2</sup>, L. Turko <sup>18</sup>, T.S. Tveter <sup>10</sup>, M. Unger <sup>4</sup>, M. Urbaniak <sup>16</sup>, D. Veberič <sup>4</sup>, O. Vitiuk <sup>18</sup>, V. Volkov <sup>20</sup>, A. Wickremasinghe <sup>22</sup>, K. Witek <sup>15</sup>, K. Wójcik <sup>16</sup>, O. Wyszynski <sup>11</sup>, A. Zaitsev <sup>20</sup>, E. Zhrebtsova <sup>18</sup>, E.D. Zimmerman <sup>24</sup>, and A. Zviagina <sup>20</sup>

<sup>1</sup> National Nuclear Research Center, Baku, Azerbaijan

<sup>2</sup> Faculty of Physics, University of Sofia, Sofia, Bulgaria

<sup>3</sup> LPNHE, Sorbonne University, CNRS/IN2P3, Paris, France

<sup>4</sup> Karlsruhe Institute of Technology, Karlsruhe, Germany

<sup>5</sup> HUN-REN Wigner Research Centre for Physics, Budapest, Hungary

<sup>6</sup> Eötvös Loránd University, Budapest, Hungary

<sup>7</sup> Institute for Particle and Nuclear Studies, Tsukuba, Japan

<sup>8</sup> Okayama University, Japan

<sup>9</sup> University of Bergen, Bergen, Norway

<sup>10</sup> University of Oslo, Oslo, Norway

<sup>11</sup> Jan Kochanowski University, Kielce, Poland

<sup>12</sup> Institute of Nuclear Physics, Polish Academy of Sciences, Cracow, Poland

<sup>13</sup> National Centre for Nuclear Research, Warsaw, Poland

<sup>14</sup> Jagiellonian University, Cracow, Poland





<sup>15</sup> AGH University of Krakow, Cracow, Poland

<sup>16</sup> University of Silesia, Katowice, Poland

<sup>17</sup> University of Warsaw, Warsaw, Poland

- <sup>18</sup> University of Wrocław, Wrocław, Poland  
<sup>19</sup> Warsaw University of Technology, Warsaw, Poland  
<sup>20</sup> Affiliated with an institution covered by a cooperation agreement with CERN  
<sup>21</sup> University of Belgrade, Belgrade, Serbia  
<sup>22</sup> Fermilab, Batavia, USA  
<sup>23</sup> University of Notre Dame, Notre Dame, USA  
<sup>24</sup> University of Colorado, Boulder, USA  
<sup>25</sup> University of Hawaii at Manoa, Honolulu, USA  
<sup>26</sup> University of Pittsburgh, Pittsburgh, USA

## The NA61/SHINE Limited Members

T. Antičić <sup>1</sup>, J.J. Back<sup>3</sup>, A. Bravar<sup>8</sup>, N. Charitonidis<sup>9</sup>, A. De Roeck<sup>9</sup>, F. Diakonov<sup>2</sup>, S.J. Dolan<sup>9</sup>, R.A. Fernandez<sup>9</sup>, K.J. Floethner<sup>9</sup>, P. Ghosh<sup>4</sup>, P. Granger<sup>9</sup>, A. Kapoyannis<sup>2</sup>, J.F. Krizmanic <sup>4</sup>, M.O. Kuttan<sup>5</sup>, F. Lanni<sup>9</sup>, O. Linnyk<sup>5</sup>, L. Munteanu<sup>9</sup>, C. Mussolini<sup>9</sup>, J. Pawlowski<sup>5</sup>, W. Rauch<sup>6</sup>, L. Scharenberg<sup>9</sup>, S. Schramm<sup>5</sup>, J. Steinheimer-Froschauer<sup>5</sup>, H. Stoecker<sup>5</sup>, H. Ströbele<sup>7</sup>, T. Šuška <sup>1</sup>, A. Toia <sup>7</sup>, M. Vassiliou<sup>2</sup>, and K. Zhou<sup>5</sup>

- <sup>1</sup> Ruđer Bošković Institute, Zagreb, Croatia  
<sup>2</sup> University of Athens, Athens, Greece  
<sup>3</sup> University of Warwick, Warwick, Great Britain  
<sup>4</sup> Goddard Space Flight Center, Greenbelt, USA  
<sup>5</sup> Frankfurt Institute for Advanced Studies, Frankfurt, Germany  
<sup>6</sup> Fachhochschule Frankfurt, Frankfurt, Germany  
<sup>7</sup> University of Frankfurt, Frankfurt, Germany  
<sup>8</sup> University of Geneva, Geneva, Switzerland  
<sup>9</sup> CERN, Geneva, Switzerland

# 1 Introduction

This annual report presents the status and plans of the NA61/SHINE experiment [1] at the CERN SPS. The report refers to the period December 2023 – November 2024.

The document is organized as follows. A summary of the 2023 and 2024 data-taking campaigns is given in Section 2. The facility status is given in Section 3. Software and calibration upgrades are summarized in Section 4. New results are presented in Section 5. The beam request for 2025 and plans for data taking in 2026 are presented in Section 6. The summary in Section 7 closes the paper.

The NA61/SHINE Collaboration submitted an addendum to the NA61/SHINE proposal to the SPS Committee in the reported period [2]. It requests a proton beam at 300 GeV/c in 2025 the cosmic-ray programme of NA61/SHINE. In addition, we submitted a memorandum requesting the use of the test beam time for physics data taking on  $\pi$ +C interactions at 158 GeV/c motivated by the studies of charge symmetry violation [3]. This data-taking was approved and successfully conducted in October 2024.

## 2 Data-taking summary

### 2.1 Neutrino-related physics run, summer 2024

The NA61/SHINE experiment acquired data using secondary protons at a momentum of 120 GeV/c over a four-week period in July 2024 with a 150-cm-long LBNF/DUNE prototype target made of IG510 graphite. Throughout most of the data acquisition phase, all TPCs and Time-of-Flight detectors were functional, with the exception of the PSDs, which are not essential for measurements related to neutrino physics. Additionally, a specialized time projection chamber called the Long Target Tracker (LTT) was developed and implemented to address the challenges associated with forward track extrapolation. Details of the LTT are presented in Section 3.2. Similar to the neutrino-related data collection in 2023, delay wire chambers were borrowed from the CERN Beams Department (BE) to serve as NA61/SHINE's Beam Position Detectors (BPD). The first 10 days were devoted for the LTT's commissioning, experimental startup, and the collection of special calibration data. The remaining approximately 2.5 weeks of beam time were dedicated to studying proton interactions at 120 GeV/c with the LBNF prototype target. The initial physics run commenced with settings at half magnetic field ("80 GeV/c " field) and transitioned to full magnetic field settings ("158 GeV/c " field) after 10 days. The recorded dataset consists of 124.7 million and 114.3 million proton interactions on the LBNF prototype target, respectively, for the two magnetic field settings. Figure 1 illustrates the experimental setup positioned in front of the NA61/SHINE main detector.

### 2.2 Strong interactions physics runs, autumn 2024

On October 31, 2024, the Pb beam at a momentum of 150A GeV/c was delivered to the NA61/SHINE experiment. After five days of setup, the production data taking started with a 3 mm lead target, providing 6% interaction probability. The data were taken with the minimum bias interaction T2 trigger and with beam T1 trigger scaled down by a factor of 100, resulting in the data sample consisting of around 8% of T1 (beam) triggers and 92% of T(interaction) triggers. The sub-systems used in this data-taking were Beam Position Detectors (BPD-1 and BPD-3), Time Projection Chambers (VTPCs and MTPCs), the Trigger and Data Acquisition system (TDAQ), the upgraded Vertex Detector (VD), the Time-of-Flight- Left (ToF-L), and the Forward Projectile Spectator Detector (FPSD). The data-taking rate with the upgraded NA61/SHINE detector is 1.2 kHz over 8.5 s SPS spill in 2023. Upgrades of the detector, combined with optimization of the SPS slow extraction, resulted in increased

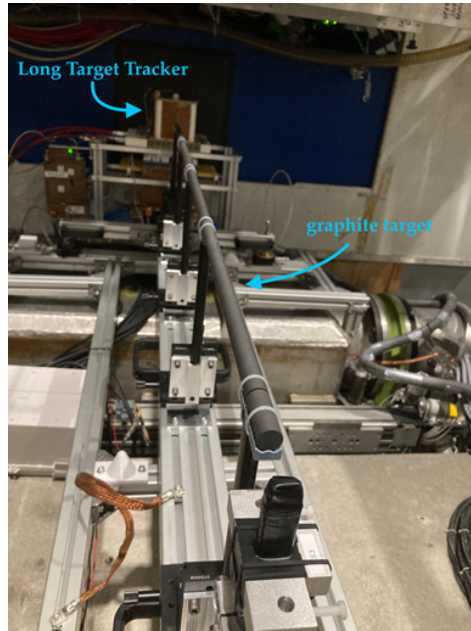


**Figure 1:** Experimental configuration of the LBNF/DUNE prototype target and LTT apparatus.

data-taking efficiency with respect to 2018 Pb data-taking by a factor of about 30. The total number of interaction trigger events collected during four calendar weeks of the Pb period amounts to about 300 million. This includes about 150 million Pb+Pb collisions. Thus, with 30 million collisions taken in 2022, and 150 millions collected in 2024 NA61/SHINE has recorded about 180 million collisions for open charm physics. The goal of 500 million events should be reached, assuming in total of seven weeks of the Pb beam in 2024 and 2025 with the planned increased efficiency of the interaction trigger. The last week of the Pb run in 2024 will be dedicated to data taking with a fragmented Pb beam at 13.5  $A$  GeV/ $c$  for cosmic ray physics.

In October 2024 the NA61/SHINE also measured of  $\pi^+ + C$  and  $\pi^- + C$  interactions at 158 GeV/ $c$  [3]. This new data will help understand the recent unexpected NA61/SHINE observation - the large violation of isospin (flavour) symmetry in the kaonic sector of multi-particle production and also results in new precision data for understanding cosmic-ray-induced air showers. During the measurements, around 30 million events were collected for each reaction.

### 3 Facility status

Before summer of 2024 the NA61/SHINE spectrometer was prepared for the data taking with the prototype DUNE target. That involved installation of the 150 cm long graphite target itself and the Long Target Tracker. During data taking the Beam Position Detectors were replaced by Delay Wire Chambers (DWCs) [4] - a standard beam instrumentation device widely used in CERN's East and North area beamlines. DWCs were installed in the same positions as BPDs. A scheme of the NA61/SHINE detector with the above additions is shown in Fig. 2.

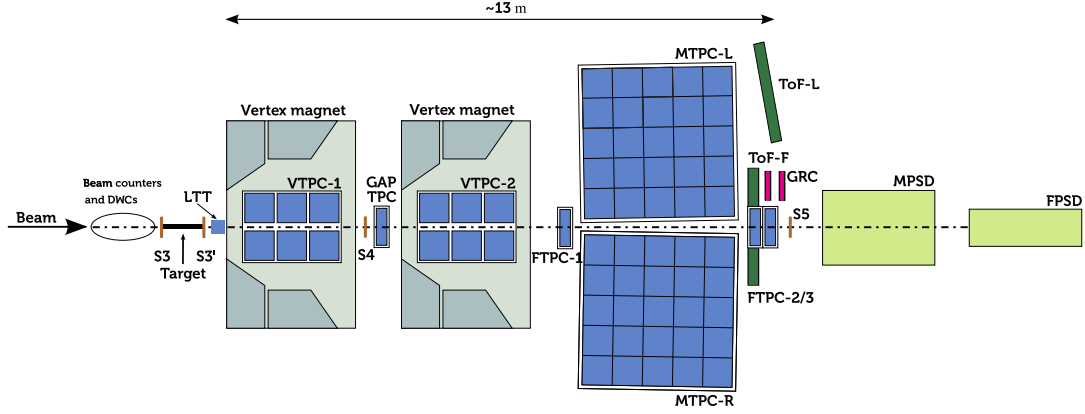


Figure 2: The layout of the NA61/SHINE detector.

### 3.1 Prototype DUNE long target

A dedicated effort was made to enable the installation and precise alignment of the prototype neutrino production target for Fermilab’s LBNF/DUNE neutrino beamline. The target, provided by the Rutherford Appleton Laboratory (United Kingdom), was composed of five cylindrical sections of IG510 graphite, each with a diameter of 16 mm, totaling a length of 150 cm. A custom target holder structure, built from Bosch Rexroth profiles, was designed in two parts: a permanently fixed bottom frame attached to the NA61/SHINE detection setup and a removable top frame that held the graphite rods forming the target. These graphite rods were supported by a lightweight carbon fiber pillar structure to minimize material budget and particle interactions. For precise rod positioning, 3D-printed seats provided secure and accurate support. High-precision kinematic mounts connected the top and bottom frames, enabling repeatable and accurate alignment of the target with respect to the beam and global coordinate system. A specialized survey by the CERN geometry team achieved sub-millimeter accuracy in positioning the assembly. Additionally, two scintillators, each with a diameter of 12 mm, were positioned directly before and after the target to verify alignment accuracy, which met the available precision standards. Dedicated datasets were also collected for background studies, with the target and top frame removed from the beamline.

### 3.2 Long Target Tracker

A significant portion of the 2024 data taking period was dedicated to the long-baseline neutrino reference measurements. These campaigns involved long-target studies, the target length being 150 cm. Simulations showed that extrapolation backwards to the target surface is fairly uncertain due to the distance to the first tracking device (VTPC1). Therefore, a special tracking station was developed for this particular run. Since the tracking station was to be directly placed downstream of the target, simulation studies showed that the typical track separation is rather small, down to the mm level. Therefore, a decent two-track resolution ( $\sim$ mm) was needed. Due to the available development time frame and budget, a natural choice was a small sized TPC chamber (10cm  $\times$  12cm  $\times$  20cm). In order to achieve a small cluster size, micropattern gas multiplication technologies (GEM) were considered.



However, the NA61/SHINE readout is only capable of sensing positive charges, as it was optimized for multi-wire proportional chamber (MWPC) based gas amplification. In order to mitigate this issue, a micropattern-inspired MWPC technology was used, called the close-cathode chamber (CCC) [5].

In the top left panel of Fig. 3 the installed detector, called the Long-Target Tracker (LTT) is shown in its final position along with the long target. In the top right panel, a typical event is seen. In the bottom left panel, a slice of the same typical event in the padrow - drift time plane is seen. The performance of the chamber in terms of cluster size and expected two-track resolution is shown in bottom right panel.

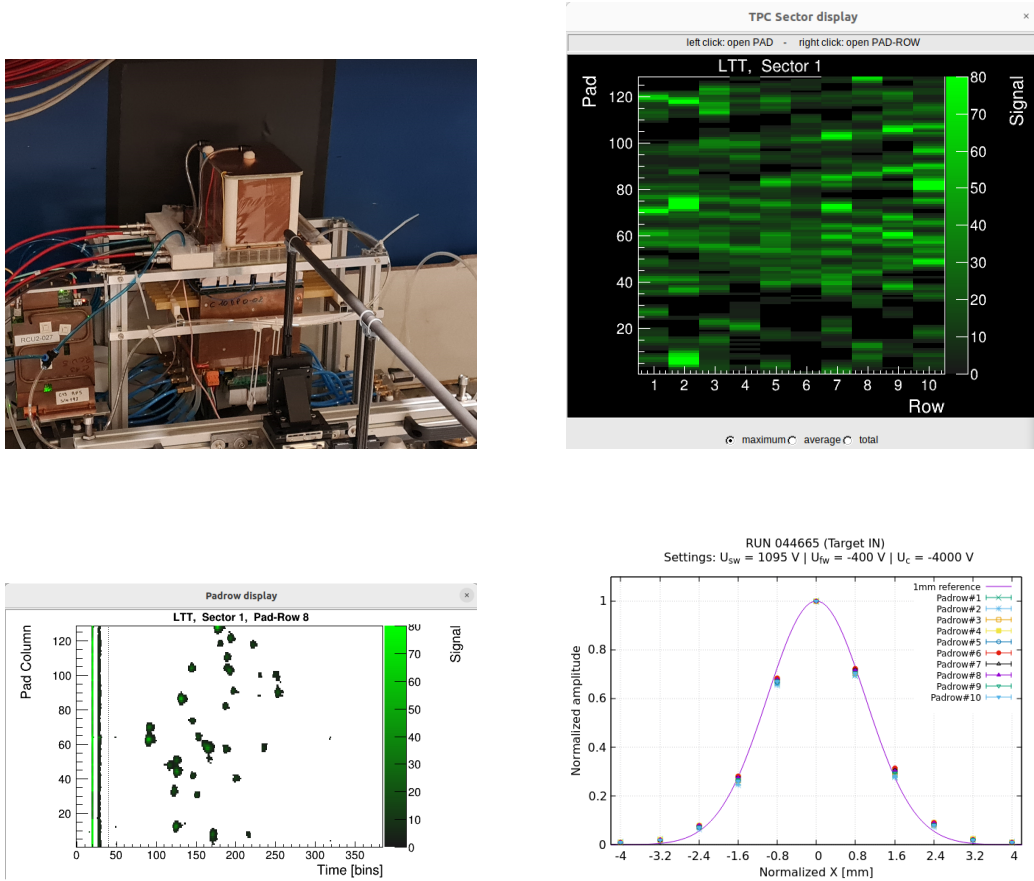


**Figure 3:** Top left: the photo of the installed Long Target Tracker (LTT) along with the LBNF graphite long target prototype, during the 2024 data taking period. Top right: raw event display of the LTT during a typical high-intensity target-in run. Bottom left: a slice of the pertinent raw event along the padrow - drift time plane. Bottom right: mean shape of the cluster profile of clusters fitted to track, in LTT. The cluster profile shape sigma is below mm level, providing a mm level two-track resolution.



## 4 Software and calibration status

### 4.1 Software

During the reporting period again software work has been steadily progressing. Main efforts were dedicated to support reconstruction, calibration, and quality monitoring of the data collected after the LS2 and the detector upgrade.

#### 4.1.1 Offline software

As was already described in the previous report, [SHINE](#), the offline software framework of the experiment, is in a longer-than-standard time between regular releases. The needs of productions for pre-LS2 data (both experimental and Monte Carlo) are covered with patch releases to the last stable release v1r21, while development continues on the v1r22 version. The latter is meant to support the post-LS2 data processing mentioned above, improve tests coverage, as well as revise core framework components along with the calibration database structure, utilizing the understanding that we have gathered over the years. The purpose of this effort is to prevent [SHINE](#) from becoming a “legacy” software and make it easier for new developers to join the work and for the users to utilize the software, solving some long-standing problems.

Since the previous report, two new patch releases of the v1r21 version were deployed. The changes included improvements in the TOF reconstruction, GEANT4 support, and most importantly transition to Alma 9 and gcc 12 compiler on lxplus/lxbatch and GitLab CI. Also two so-called release candidates of the developing v1r22 version were prepared. These are installations on cvmfs to support data taking and calibration for the newly collected data, but are not kept compatible with the developing calibration database structure beyond their temporary use.

Some of the changes to the offline software in the v1r22 version and the associated infrastructure, are listed below.

- (i) With the transition to Alma 9, the build farm was updated not only to the new operating system, but also using machines with two times more cores, thus providing significantly faster feedback to the developers.
- (ii) A configuration file for clang-format was created to facilitate following [SHINE](#) coding conventions to improve readability of out codes.
- (iii) A new framework for integration/validation tests was deployed. The system is built around the shellspec shell testing framework and ctest that we have already used to drive unit tests. It allows for proper integration with GitLab UI, parallelization and standardization of tests, and running tests for any choice of optional components of [SHINE](#) in the build. The latter allowed to cover e.g. Monte Carlo applications, that were not covered until now.
- (iv) Legacy part of the database was finally frozen. This part, associated with the so-called “Legacy” software in [SHINE](#), the software inherited from the NA49 experiment, used to be updated in synchronization with the “native” database giving space to errors. Now all the information is coming solely from the “native” part and is fed into “Legacy” software if needed.
- (v) Utilities were added to further streamline implementation and testing of managers. They are classes that are responsible for reading in detector-related information from the database and other sources, that are undergoing a significant revision in the v1r22 version.

- (vi) Progress was made in understanding of problems with the native tracking for high multiplicity data and workarounds were developed. Also detailed measures of tracking performance were developed along with associated tools and testing scheme to facilitate further development.
- (vii) Work is ongoing on improving the overly-simplistic native TPC clusterization algorithms.
- (viii) Multiple bugs were squashed.

Apart from the above, AI tools are being developed to filter out noise clusters. This may improve performance of tracking, especially in the context of online QA, where speed is crucial, while some accuracy can be sacrificed. Furthermore, a new analysis framework, SANE, was proposed to among others standardize data filtering (cuts) procedures and accumulation parts of analyses. In this context “analysis” is meant as anything that reads events and gets some information out of them, without changing the events. This includes QA, calibration and physics analysis.

#### 4.1.2 Online software

The core of the data acquisition (DAQ) system was migrated to the *DAQling* software framework. The initiative for the migration came from the CERN EP-DT-DI department. Until recently, the framework was only used by one other small size experiment, FASER, and integration into the NA61/SHINE experiment would both help with the popularization and stimulate improvements of the framework to meet the requirements of the NA61/SHINE DAQ system. During the integration into our DAQ system, the framework performance in terms of data throughput was improved, and new monitoring-related features were introduced. During the migration, major portion of the NA61/SHINE DAQ code was revived and adjusted when necessary, resulting, for instance, in improvement of code-guards to ensure the data integrity. Changes in the core framework also triggered the development of a new Python interface for the process-pool management. The new interface is an improvement upon both the one previously used by the NA61/SHINE DAQ and the native interface shipped with the *DAQling* framework by providing strict synchronization points, allowing strict control over the state of the process-pool, and easy-to-use yet robust API reducing margins for errors in the DAQ control applications.

Online quality assessment (QA) system was upgraded to handle high data loads without tradeoff in responsiveness. The preparation of the QA report is done in two formal stages: 1) many independent instances of the reconstruction software, SHINEOFFLINE, are analysing the incoming data and filling in the necessary histograms; 2) central “QACollector” process is polling these instance, accumulates ROOT files with the histograms, merges them together, and the result is then sent to the front-end GUI. The bottleneck of the system for the previous runs was the merging of ROOT files. It was surpassed by introduction of dedicated system capable of parallelizing the merging over (potentially) unlimited number of machines, and, in turn, allowing for implementation of logarithmic scalability of the system w.r.t. the load put on the system. After the upgrade, the system was able to consistently produce up-to-date QA reports with  $\approx 1$  minute intervals, processing 100% of the recorded events, while working on close to maximal load expected at our experiment.

## 4.2 Calibration

Calibration activities and upgrades performed during the last year are the following:

- (A) Generally for the post-LS2 data sets

- (i) An instrumentation paper [6] was written and published about the TPC geometry calibration strategy and procedure, primarily describing our new Geometry Reference Chamber (GRC), its design concept, usage and performance. Moreover, the paper also describes the TPC geometry calibration in a broader context.
- (B) Concerning Pb+Pb collisions at 150A GeV/c collected in 2022 and 2023
- (i) Calibration of the timing reference detectors and TPC start time performed and in DB (Stage1a, Stage1b).
  - (ii) Revision and cross-checks for the large TPCs (VTPC1, VTPC2, MTPCL, MTPCR) alignment calibration.
  - (iii) Revision and cross-checks for the large TPCs (VTPC1, VTPC2, MTPCL, MTPCR) start time ( $t_0$ ) and drift direction displacement ( $y_0$ ) calibration.
  - (iv) Getting ready for large scale production for drift velocity refined calibration (Stage2).
  - (v) Developed alignment calibration procedure for Vertex Detector (VD) versus TPC system alignment.
- (C) Concerning 2022, 2023 neutrino-related data
- (i) Calibration of the timing reference detectors and TPC start time performed and in DB (Stage1a, Stage1b).
  - (ii) Alignment calibration of the small TPCs (GTPC, FTPC1, FTPC2, FTPC3) started.
  - (iii) Beam Position Detector (BPD) alignment calibration started.
- (D) Concerning data collected prior to detector upgrade
- (i) the energy loss ( $dE/dx$ ) was calibrated using the new SHINE software procedure for  $p+p$  at 158 GeV/c collected in 2010 which improved particle identification precision. The new production of the sample was prepared.
  - (ii) the SHINE calibration software for  $dE/dx$  was applied for XeLa data samples using also cut on the track multiplicity if needed (beam momentum 75 GeV/c and 150 GeV/c) . The final productions were prepared.
  - (iii) after finishing VTPC and MTPC calibration, i.e. drift velocity ( $v_{drift}$ ), time constants, and geometrical corrections, for  $p+p$  at 400 GeV/c data sample the residual corrections for cluster positions were calculated and applied. The BPD position corrections using BPD-TPC alignment were obtained and included in the Data Base.

#### 4.2.1 Calibration of internal Vertex Detector geometry

The alignment of VD sensors was done using track candidates found by the combinatorial method with data taken with-out magnetic field during Pb run in 2022. The procedure was very similar to that used for the pilot version of vertex detector SAVD which is described in details in [7] in sec. 4.2 and in [8]. Because VD contains much more sensors (64) as compared to SAVD (16) the number of 3 sensor combinations (listed in [8] for SAVD) increased significantly and a dedicated C++ method was involved to handle this combinations in the minimization MINUIT package. In addition, the minimization procedure was split to 3 iterative steps to limit a number of search parameters in MINUIT.

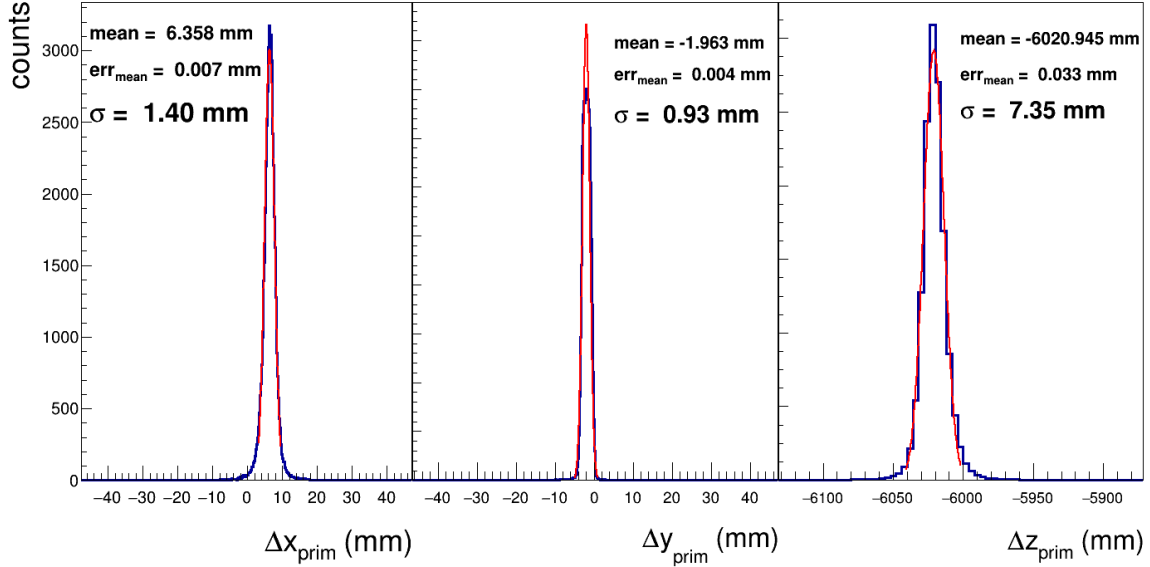


**Figure 4:** The distributions of between the positions of reconstructed primary vertices in the VD and the TPCs in a given event in the  $x$  (*left*),  $y$  (*middle*) and  $z$  (*right*) coordinate, respectively. The mean values take from the Gaussian fit to the distributions are used as relative VD-TPC position calibration parameters.

#### 4.2.2 Alignment of Vertex Detector with TPCs

The multiplicities of VD and TPC tracks are well correlated, proving that the tracking procedures used are correct. It may be observed that for some events, tracks were reconstructed in either VD or TPCs, but not both. These cases are related to low-track multiplicity events selected by the minimum bias trigger. Merging the track fragments measured by VD and TPCs requires the VD alignment relative to the TPCs. By observing the difference between the positions of reconstructed primary vertices in the VD and the TPCs in a given event, the VD position can be calibrated with an accuracy of  $7\ \mu\text{m}$ ,  $4\ \mu\text{m}$  and  $33\ \mu\text{m}$  in the  $x$ ,  $y$  and  $z$  coordinate, respectively. The distributions of the respective differences are show in Fig. 4 for events having VD track multiplicities in the range from 20 to 350. This is a typical selection used for early analyses of Pb+Pb data take in 2022 due to a strong inefficiency of TPC tracking at higher track multiplicities.

## 5 New results

### 5.1 New results for strong interaction physics

The NA61/SHINE strong interaction program is based on beam momentum scans ( $13A-150A/158A\ \text{GeV}/c$ ) with light and intermediate-mass nuclei (from  $p+p$  to  $\text{Xe}+\text{La}$ ). The main physics goals include search for the critical point of strongly interacting matter and study the properties of the onsets of deconfinement and fireball. The program has been extended in recent years by Pb+Pb collisions, where the open charm production and collective effects are studied.

This section summarizes new preliminary and recently published physics results from the program on the physics of strong interactions. The results on spectra and yields, as well as on fluctuations and correlations, are presented. They are labeled according to the NA61/SHINE physics goals, i.e., the

study of the onsets of deconfinement (OD) [9] and fireball (OF) [10], the search for the critical point (CP), and others (O).

### 5.1.1 (OD, OF) Published results on $\pi^\pm$ , $K^\pm$ , $p$ , and $\bar{p}$ production in 0–10% central Ar+Sc collisions at 13A–150A GeV/c

The results on  $\pi^\pm$ ,  $K^\pm$ ,  $p$ , and  $\bar{p}$  spectra and yields in 0–10% central Ar+Sc collisions at 13A, 19A, 30A, 40A, 75A, and 150A GeV/c beam momenta ( $\sqrt{s_{\text{NN}}} = 5.1, 6.1, 7.6, 8.8, 11.9, \text{ and } 16.8$  GeV) were published in Eur. Phys. J. C [11]. The double-differential distributions  $d^2n/dydp_T$  as well as rapidity spectra  $dn/dy$  as are presented. The mean multiplicities were obtained from the integrated rapidity distributions. The example yield ratios are presented in Sec. 5.1.10 (Fig. 16) together with new preliminary Xe+La results.

### 5.1.2 (O, OD) Submitted results on $K_S^0$ meson production in 0–10% central Ar+Sc collisions at 75A GeV/c

The NA61/SHINE paper showing the evidence for an unexpected excess of charged over neutral  $K$  mesons (possible evidence of isospin-symmetry violation) in Ar+Sc collisions at 75A GeV/c ( $\sqrt{s_{\text{NN}}} = 11.9$  GeV) was submitted to the *Nature Physics* (preliminary results were presented in the last Status Report). Soon after, the editor of the *Nature Physics* suggested that the *Nature Communications* would be more in line with the content of the paper. The same path was followed by an independent phenomenology paper [12] attempting to explain the excess reported by NA61/SHINE. After receiving the reviewers' comments, the editor of the *Nature Communications* suggested merging the two publications. The merged paper [13], with the author list expanded, has been just re-submitted to the *Nature Communications*. The reviewers' comments from both papers were included in the combined paper. The *reply letter* contains detailed responses to all six reviewers' questions.

### 5.1.3 (CP) Published results on higher-order moments of multiplicity and net-electric charge distributions in inelastic $p+p$ collisions at 20–158 GeV/c

The results on higher-order moment fluctuations in inelastic  $p+p$  collisions at 20, 31, 40, 80, and 158 GeV/c beam momenta ( $\sqrt{s_{\text{NN}}} = 6.3, 7.7, 8.8, 12.3, \text{ and } 17.3$  GeV) were published in Eur. Phys. J. C [14]. Pure moments are sensitive to the system size so the ratio of cumulants is used to search for physics phenomena, in particular, the CP signal [15, 16]. In the case of positively ( $[h^+]$ ) and negatively ( $[h^-]$ ) charged hadrons as well as their sum  $[h^+ + h^-]$ , one considers ratios of  $\kappa_2/\kappa_1$  (scaled variance),  $\kappa_3/\kappa_2$  (scaled skewness), and  $\kappa_4/\kappa_2$  (scaled kurtosis) which can be directly compared between different systems (reference value of 1 is defined by the Poisson distribution). In case of net-electric charge ( $[h^+ - h^-]$ ) the first two ratios are slightly modified to keep the reference value (1 for the Skellam distribution):  $\kappa_2[h^+ - h^-]/(\kappa_1[h^+] + \kappa_1[h^-])$ ,  $\kappa_3/\kappa_1[h^+ - h^-]$ . The examples of obtained results are shown in Fig. 5. One can observe general agreement with the models.

Utilizing intensive quantities one can qualitatively compare the published results with the signal measured by the STAR experiment [18] (see Fig. 6). Except the second cumulant ratio there is a general agreement between both reactions but one should keep in mind differences in considered phase space as well as volume fluctuations in Au+Au.

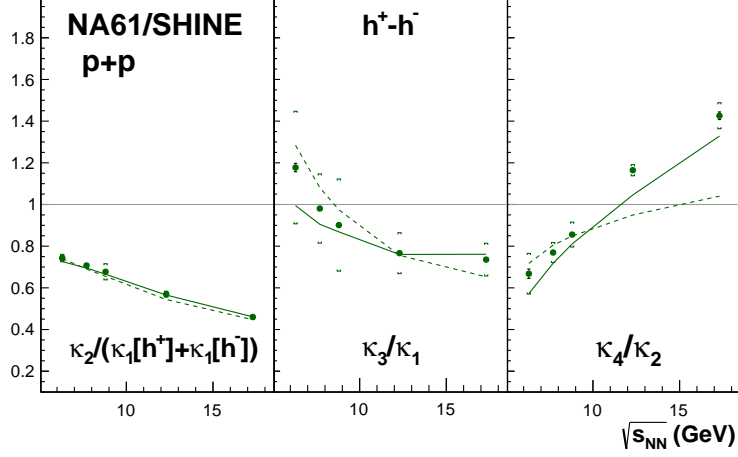


**Figure 5:** Published NA61/SHINE results on energy dependence of intensive quantities of net-electric charge distribution in  $p+p$  interactions at  $\sqrt{s_{NN}} = 6.3, 7.7, 8.8, 12.3,$  and  $17.3$  GeV in the phase-space region as defined in Ref. [17]. The statistical uncertainty is indicated with a color bar (often smaller than the marker), and systematic uncertainty is indicated with a square bracket. Results are compared with EPOS1.99 (solid line) and FTTP-BERT (dashed line) predictions.

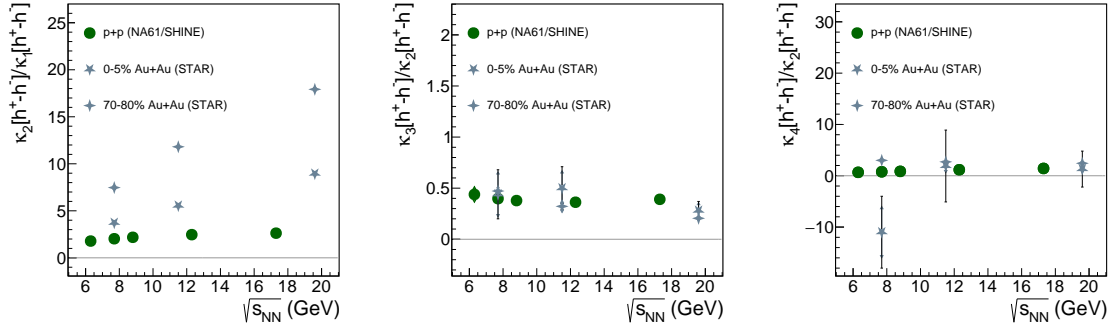


**Figure 6:** Published results on net-electric charge cumulant ratios measured in  $p+p$  interactions by NA61/SHINE and in central and peripheral Au+Au interactions by STAR [18].

#### 5.1.4 (CP) Published results on proton intermittency in 0–10% central Ar+Sc collisions at 13A–75A GeV/c

The results on proton intermittency in 0–10% central Ar+Sc collisions at 13A, 19A, 30A, 40A, and 75A GeV/c beam momenta ( $\sqrt{s_{NN}} = 5.1, 6.1, 7.6, 8.8,$  and  $11.9$  GeV) were published in Eur. Phys. J. C [19]. This analysis examined the behavior of the second-order scaled factorial moment of the proton multiplicity distribution,  $F_2(M)$ , with the increasing number of cells ( $M^2$ ) in transverse momentum. The scaled factorial moment of the order  $r$  is defined as:

$$F_r(M) = \frac{\left\langle \frac{1}{M^2} \sum_{m=1}^{M^2} n_m(n_m-1)\dots(n_m-r+1) \right\rangle}{\left\langle \frac{1}{M^2} \sum_{m=1}^{M^2} n_m \right\rangle^r}, \quad (1)$$

where  $n_m$  denotes the number of particles in the  $m$ -th bin in  $p_x$ - $p_y$  plane, and  $\langle \dots \rangle$  denotes averaging over events. When the system freezes out at CP, the scaled factorial moments  $F_r(M)$  are expected to follow a power-law behavior:  $F_r(M) \sim (M^2)^{\phi_r}$ . For protons and  $r = 2$ ,  $\phi_2 = 5/6$  is expected [20].

In order to eliminate the (trivial) dependence of  $F_2(M)$  on the shape of the single-particle transverse momentum distribution, its components,  $p_x$  and  $p_y$ , have been transformed into their cumulative equivalents [21]. Moreover, the  $F_2(M)$  values for different  $M^2$  are statistically independent, as each data point was calculated using a separate sub-sample of available events. The dependence of the second-order scaled factorial moment of proton multiplicity distribution at mid-rapidity on the number of subdivisions in cumulative transverse momentum space is shown in Fig. 7. The results show no intermittency signal. The ongoing critical point search studies via proton intermittency are summarized on the diagram of chemical freeze-out temperature and baryon-chemical potential (estimated based on Ref. [22]) and shown in Fig. 8.

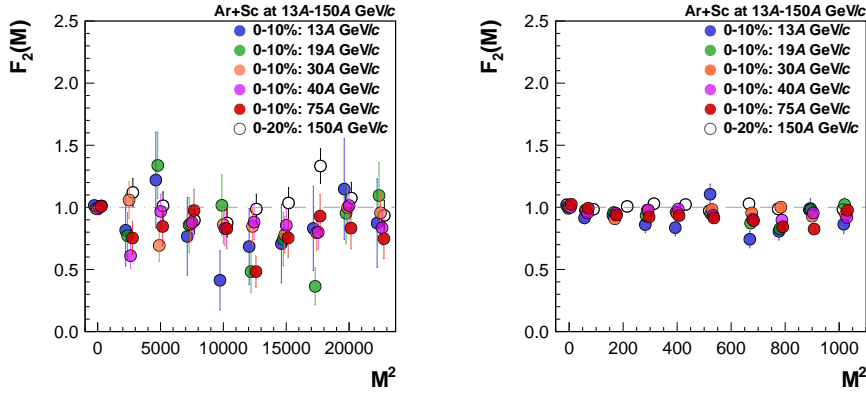


**Figure 7:** Summary of published proton intermittency results from NA61/SHINE Ar+Sc energy scan. Results on the dependence of the scaled factorial moment of proton multiplicity distribution on the number of subdivisions in cumulative transverse momentum space  $M^2$  for  $1^2 \leq M^2 \leq 150^2$  (left) and  $1^2 \leq M^2 \leq 32^2$  (right) are shown. The open circles represent results on 0–20% central Ar+Sc collisions at 150A GeV/c [23]. Closed circles indicate the most recent results for 0–10% central Ar+Sc collisions at 13A, 19A, 30A, 40A, and 75A GeV/c [19]. Points for different energies are slightly shifted in the horizontal axis to increase readability.

### 5.1.5 (O, OD) Published results on $K_S^0$ meson production in inelastic $p+p$ collisions at 31, 40, and 80 GeV/c

The results on  $K_S^0$  meson spectra and yields in inelastic  $p+p$  collisions at 31, 40, and 80 GeV/c beam momenta ( $\sqrt{s_{NN}} = 7.7, 8.8, \text{ and } 12.3 \text{ GeV}$ ) were published in Eur. Phys. J. C [25]. The double-differential distributions  $d^2n/dydp_T$  as well as rapidity spectra  $dn/dy$  as are presented. The mean multiplicities were obtained from the integrated rapidity distributions. The results are compared with predictions of microscopic models and with world  $p+p$  data at a similar energy range.

### 5.1.6 (O, CP) Preliminary results on femtoscopy analysis in 0–10% central Ar+Sc collisions at 13A–75A GeV/c

The first preliminary results on femtoscopy analysis in 0–10% Ar+Sc collisions at 150A GeV/c were presented in Ref. [26]. The new results in 0–10% Ar+Sc collisions at 40A GeV/c and 75A GeV/c were



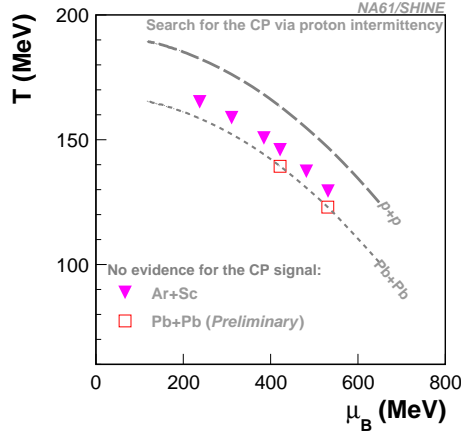


**Figure 8:** Diagram of chemical freeze-out temperature and baryon-chemical potential. The dashed line indicates parameters in  $p+p$  interactions and the dotted line in the central Pb+Pb collisions; points estimated and extrapolated ( $\mu_B$  for  $p+p$ ) based on Ref. [22]. The colored points mark reactions (Ar+Sc and Pb+Pb [24]) in the  $T - \mu_B$  phase diagram for which the search for the critical point was conducted, and no evidence for the critical point was found.

released as preliminary last year and presented in Refs. [27, 28]. The full beam momentum scan, including 13A, 19A, and 30A GeV/c data released this year, was presented in Refs. [29–34].

The nature of the quark-hadron transition can be studied via femtoscopy analysis as the investigation of the correlation functions in nucleus-nucleus reactions may reveal the space-time structure of the hadron production source. With the use of Lévy-type sources, we can describe the source parameters ( $\alpha$ ,  $\lambda$ , and  $R$ ) as a function of the average transverse mass of the pion pair [35].

At all energies, the 10% most central events were analyzed, and momentum correlations of identified pions were measured. The correlation functions could be described with the assumption of Lévy sources in a statistically acceptable manner, enabling the interpretation of the fit parameters.

The Lévy stability parameter  $\alpha$  describes the shape of the source. Furthermore,  $\alpha$  was conjectured to be related to one of the critical exponents (the so-called correlation exponent  $\eta$ ) and thus may shed light on the location of the critical end-point on the QCD phase diagram [36]. Assuming that  $\alpha$  is approximately constant with regards to transverse mass  $m_T$ , one can fit a constant to all  $m_T$  values at each energy, which results in an average  $\alpha$  shown in Fig. 9. The pion-producing source in all energies of Ar+Sc collisions appears to be compatible with the Lévy shape assumption, in most cases away from Gaussian and not at the CP (corresponding to  $\alpha = 2$  and  $\alpha \leq 0.5$ , respectively). Our new energy scan results yield values for  $\alpha$  between 1.5 and 2.0, and a hint of a non-monotonic trend appears with a minimum between 19A GeV/c and 30A GeV/c beam momenta. The numerical values of  $\langle \alpha \rangle$  (Fig. 9) in Be+Be and Ar+Sc systems are the following:  $1.07 \pm 0.06$  (stat.)  $^{+0.17}_{-0.07}$  (sys.) in Be+Be at 150A GeV/c [37] (the published result includes statistical uncertainty only; the systematic uncertainty is appended here);  $1.83 \pm 0.06$  (stat.)  $^{+0.15}_{-0.12}$  (sys.) in Ar+Sc at 150A GeV/c;  $1.601 \pm 0.05$  (stat.)  $^{+0.18}_{-0.024}$  (sys.) in Ar+Sc at 75A GeV/c;  $1.602 \pm 0.06$  (stat.)  $^{+0.07}_{-0.029}$  (sys.) in Ar+Sc at 40A GeV/c;  $1.56 \pm 0.06$  (stat.)  $^{+0.10}_{-0.14}$  (sys.) in Ar+Sc at 30A GeV/c;  $1.56 \pm 0.10$  (stat.)  $^{+0.13}_{-0.07}$  (sys.) in Ar+Sc at 19A GeV/c;  $1.90 \pm 0.18$  (stat.)  $^{+0.24}_{-0.20}$  (sys.) in Ar+Sc at 13A GeV/c.

The Lévy scale parameter  $R$  corresponds to the femtosopic scale of the system (it is related to the kind of homogeneity length). From a simple hydro picture, one obtains an  $R \propto 1/\sqrt{m_T}$  type of transverse mass dependence, creating a decreasing trend of  $R$  in  $m_T$ , generally attributed to transverse flow. Our

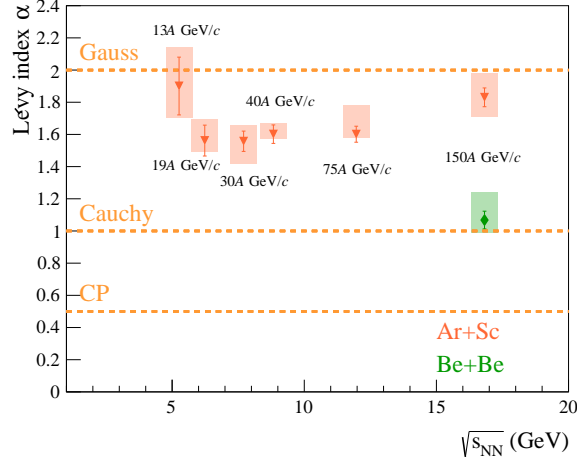


**Figure 9:** Lévy stability parameter  $\alpha$  (constant fit to all  $m_T$  values) versus energy in 0–20% central Be+Be collisions at 150A GeV/c (based on Ref. [37]) as well as in 0–10% central Ar+Sc collisions at 13A–75A GeV/c (NA61/SHINE preliminary results). The three cases for  $\alpha$  are marked and shown with dashed lines. Gaussian shape with  $\alpha = 2$ , Cauchy shape with  $\alpha = 1$ , and vicinity of the CP at  $\alpha \leq 0.5$ .

results, shown in Fig. 10, indicate that  $R$  decreases with  $m_T$ , showing a hydro-type of transverse flow effect. This is interesting in particular as we observe the described  $R \propto 1/\sqrt{m_T}$ , however, one would expect this to show only at  $\alpha = 2$  [38]; this phenomenon was also observed at RHIC [39].

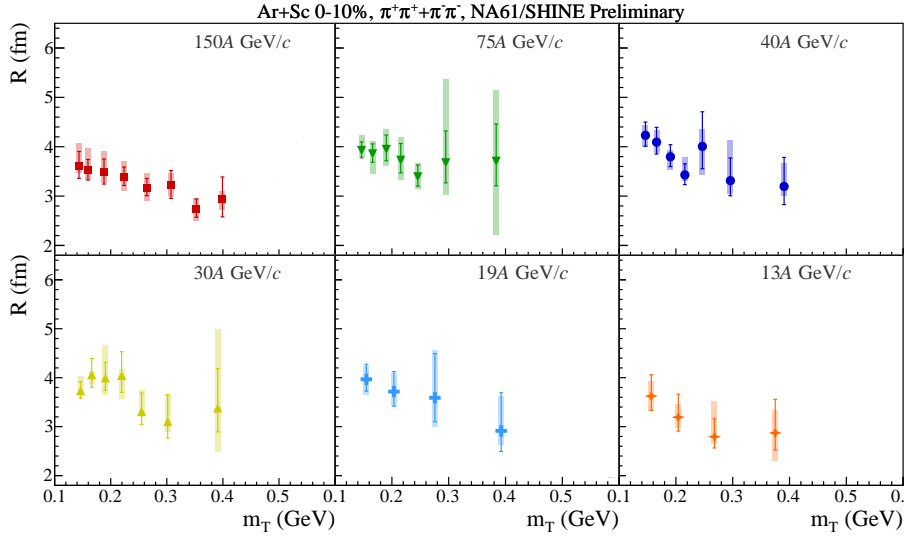


**Figure 10:** Preliminary NA61/SHINE results on Lévy scale parameter  $R$  versus  $m_T$  in 0–10% central Ar+Sc collisions at 13A–150A GeV/c.

### 5.1.7 (O) Preliminary results on $K^*(892)^0$ production in 0–10% central Ar+Sc collisions at 40A, 75A, and 150A GeV/c

The preliminary results on  $K^*(892)^0$  meson production in 0–10% central Ar+Sc collisions at 40A, 75A, and 150A GeV/c were released by NA61/SHINE and presented in Refs. [29, 31, 40–44]. Those are the first measurements of  $K^*(892)^0$  yields in intermediate-mass systems at the SPS energies. The preliminary results include transverse momentum and transverse mass spectra with inverse slope parameters, rapidity spectra, and  $K^*(892)^0$  mean multiplicities obtained in almost complete transverse momentum range ( $0 < p_T < 1.5$  GeV/c). The latter are:  $\langle K^*(892)^0 \rangle = 1.449 \pm 0.13$  (stat)  $\pm 0.079$  (sys) for Ar+Sc at 40A GeV/c,  $\langle K^*(892)^0 \rangle = 1.514 \pm 0.096$  (stat)  $\pm 0.17$  (sys) for Ar+Sc at 75A GeV/c, and  $\langle K^*(892)^0 \rangle = 2.34 \pm 0.14$  (stat)  $\pm 0.14$  (sys) for Ar+Sc at 150A GeV/c.

The analysis of  $K^*(892)^0$  resonance allows us to better understand the time evolution of high-energy nucleus-nucleus collisions. Namely, the ratio of  $K^*(892)^0$  to charged kaons is used to determine the time between chemical (end of inelastic interactions / fixing the quark composition) and thermal/kinetic (end of elastic interactions) freeze-outs [45]. These times, already estimated in central Pb+Pb/Au+Au collisions at the SPS, RHIC, and LHC energies, are at the level of a few fm/c [46–50].

Three panels of Fig. 11 (*top* and *bottom left*) show the system size dependence of  $K^*/K$  ratio at three SPS energies. The decrease of  $K^*/K$  ratio from  $p+p$  to nucleus-nucleus collisions suggests that rescattering processes play an important role in a hadronic system produced in nucleus-nucleus collisions. Following Refs. [45, 51] the lifetime of such hadronic system (time between freeze-outs) can be determined using the formula:

$$\frac{K^*}{K}|_{kinetic} = \frac{K^*}{K}|_{chemical} \cdot e^{-\frac{\Delta t}{\tau}}, \quad (2)$$

where  $\frac{K^*}{K}|_{chemical}$  can be represented by the  $K^*/K$  ratio in inelastic  $p+p$  collisions,  $\frac{K^*}{K}|_{kinetic}$  can be represented by the  $K^*/K$  ratio in nucleus-nucleus collisions,  $\tau$  is the  $K^*(892)^0$  lifetime (taken as 4.17 fm/c [52]), and  $\Delta t$  is the time between chemical and kinetic freeze-outs in nucleus-nucleus collisions (in the  $K^*$  rest frame). The obtained  $\Delta t$  values, boosted by the Lorentz factor  $\gamma = \sqrt{1 + (\langle p_T \rangle / m_0 c)^2}$  (see Ref. [53] for details), are presented in Fig. 11 (*bottom right*). The time between freeze-outs is similar for central Ar+Sc and Pb+Pb collisions at the highest energy ( $\sqrt{s_{NN}} \approx 17$  GeV). Moreover, it is also similar for Ar+Sc collisions at  $\sqrt{s_{NN}} \approx 12$  GeV and  $\sqrt{s_{NN}} \approx 17$  GeV. On the other hand, this time seems to be consistent with zero for Ar+Sc collisions at  $\sqrt{s_{NN}} = 8.8$  GeV.

### 5.1.8 (O, OD, OF) Preliminary results on $\Lambda$ production in 0–10% central Ar+Sc collisions at 40A and 150A GeV/c

The new preliminary results on  $\Lambda$  baryon production in 0–10% central Ar+Sc collisions at 40A and 150A GeV/c were released and presented for the first time in Refs. [59, 60] together with older preliminary results (75A GeV/c) already shown in Ref. [61]. The results include double-differential spectra in rapidity-transverse momentum phase space, transverse momentum spectra with inverse slope parameters, rapidity spectra, and mean multiplicities. The obtained mean multiplicities of  $\Lambda$  baryons are  $5.49 \pm 0.12$  (stat)  $\pm 0.24$  (sys) for Ar+Sc at 40A GeV/c and  $6.43 \pm 0.13$  (stat)  $\pm 0.88$  (sys) for Ar+Sc at 150A GeV/c.

The NA61/SHINE energy dependencies of the multiplicity at mid-rapidity ( $|y| < 0.5$ ) and mean multiplicity of  $\Lambda$  baryons, along with available world data, are presented in Fig. 12. Both quantities reach a plateau within the SPS energy range regardless of the collision system size. The values for Ar+Sc and Si+Si collisions are much closer to those observed in Au+Au and Pb+Pb collisions than in  $p+p$  interactions.

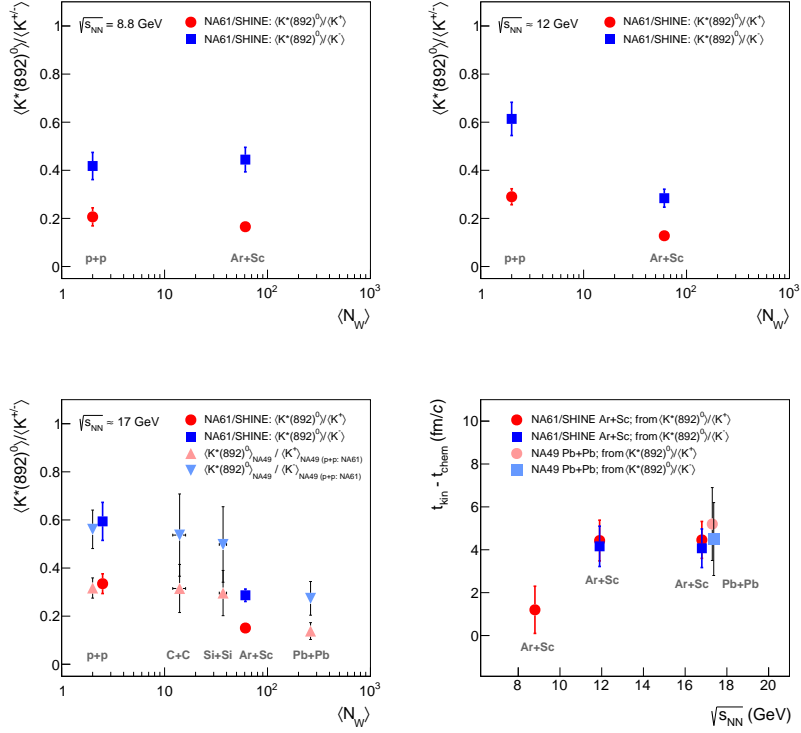


**Figure 11:** The system size dependence of  $K^*/K$  ratio at  $\sqrt{s_{NN}} = 8.8$  GeV,  $\sqrt{s_{NN}} \approx 12$  GeV, and  $\sqrt{s_{NN}} \approx 17$  GeV (top and bottom left) as well as the energy dependence of time between freeze-outs (bottom right). Plots prepared based on preliminary NA61/SHINE results on  $K^*(892)^0$  production in 0–10% central Ar+Sc collisions as well as published NA49 and NA61/SHINE results on  $K^*(892)^0$  [46, 54, 55] and  $K^{+/-}$  [11, 56–58] yields. See Ref. [46] for more details on compilation of  $K^*/K$  ratios at  $\sqrt{s_{NN}} \approx 17$  GeV.

Figure 13 illustrates the energy dependencies of the  $\langle \Lambda \rangle / \langle \pi \rangle$  ratio and total strangeness production  $E_S$ . The  $E_S$  is defined following the description in Ref. [62]:

$$E_S = \frac{\langle \Lambda \rangle + \langle K + \bar{K} \rangle}{\langle \pi \rangle}, \quad (3)$$

where  $\langle \pi \rangle$  can be taken as equal  $1.5 \cdot (\langle \pi^+ \rangle + \langle \pi^- \rangle)$ , and  $\langle \pi^+ \rangle$  and  $\langle \pi^- \rangle$  are mean multiplicities of positively and negatively charged pions, respectively. Because at the SPS energies the  $\bar{\Lambda}/\Lambda$  ratio is typically less than 0.15 [63], the  $\bar{\Lambda}$  contribution to  $E_S$  is small and therefore neglected. To include as much data as possible,  $\langle K + \bar{K} \rangle$  is expressed as  $4 \cdot \langle K_S^0 \rangle$  for  $p+p$  data and as  $2 \cdot (\langle K^+ \rangle + \langle K^- \rangle)$  for A+A data. For Au+Au and Pb+Pb collisions, both  $\langle \Lambda \rangle / \langle \pi \rangle$  ratio and  $E_S$  show a distinct maximum at middle SPS energies. A hint of such a maximum is not visible in  $E_S$  for Ar+Sc data. On the other hand, the trend of  $\langle \Lambda \rangle / \langle \pi \rangle$  ratio in Ar+Sc collisions at three studied energies is similar to the trend observed in the heavy Pb+Pb system.

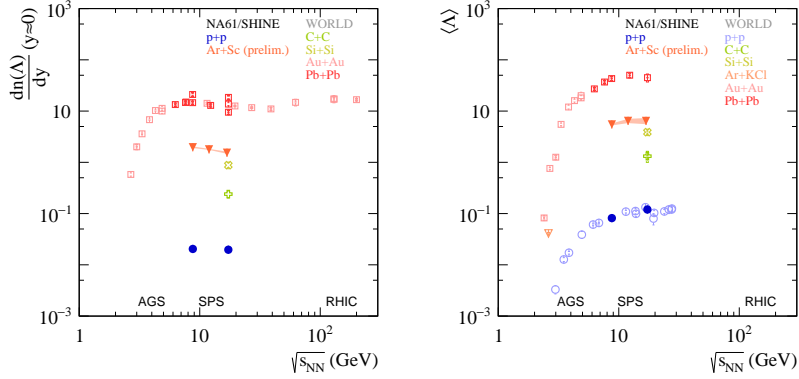


**Figure 12:** The energy dependence of mid-rapidity yield (*left*) and the mean multiplicity (*right*) of  $\Lambda$  baryons. The NA61/SHINE results on  $p+p$  at 40 GeV/c as well as Ar+Sc are preliminary, and the NA61/SHINE results on  $p+p$  at 158 GeV/c are published [64]. See Ref. [60] for the references to the world data. The systematic uncertainties of the Ar+Sc results are presented as a shaded band.

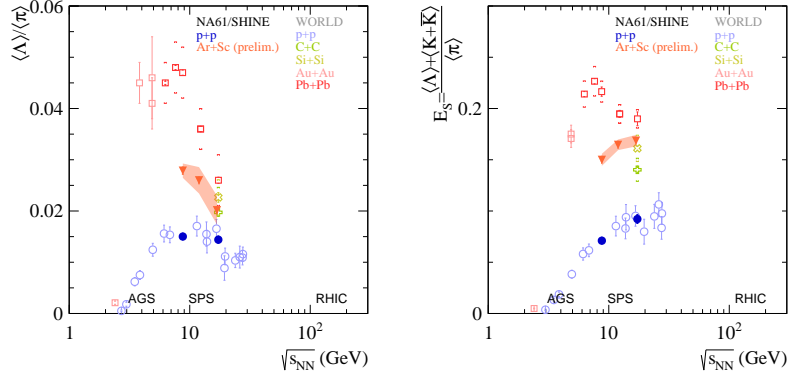


**Figure 13:** The energy dependence of  $\langle \Lambda \rangle / \langle \pi \rangle$  ratio (*left*) and total strangeness production  $E_S$  (*right*). See Ref. [60] for the references to numerical values needed to obtain the particle ratios. The systematic uncertainties of the Ar+Sc results are presented as a shaded band.

### 5.1.9 (CP) Preliminary results on $h^-$ intermittency in 0–20% central Xe+La collisions at 150A GeV/c

The preliminary NA61/SHINE results on the intermittency analysis of negatively charged hadrons produced in 0–20% central Xe+La collisions at 150A GeV/c were released recently and presented in Refs. [29, 31, 44, 65, 66]. The analysis was performed using 2nd, 3rd, and 4th-order scaled factorial moments.

The NA61/SHINE results on proton intermittency analysis were discussed in Sec. 5.1.4. In that analysis, the notation  $F_2(M)$  was used for the second-order scaled factorial moment as a function of the number of subdivisions  $M^2$  in cumulative transverse momentum space. In the  $h^-$  intermittency analysis, we use a different notation. Namely, the results are presented using  $\Delta F_r(M)_c$  ( $r = 2, 3, 4$ ) as a function of  $M^2$ . The definition is as follows:

$$\Delta F_r(M)_c = F_r(M) - F_r(1), \quad (4)$$

where  $F_r(M)$  and  $F_r(1)$  are also computed by employing the cumulative  $p_T$  binning. Note that  $F_r(1) = F_r(M)$  for uncorrelated particles in  $p_T$ .

In this analysis, the scaled factorial moments of negatively charged hadron multiplicities were studied. However, the significantly higher number of produced negatively charged hadrons, compared to protons, allowed this analysis to be performed up to the 4th-order scaled factorial moment. The results are presented in Fig. 14. No signs of  $\Delta F_r(M)_c$  increase with  $M^2$  are observed in any order of the studied scaled factorial moments.

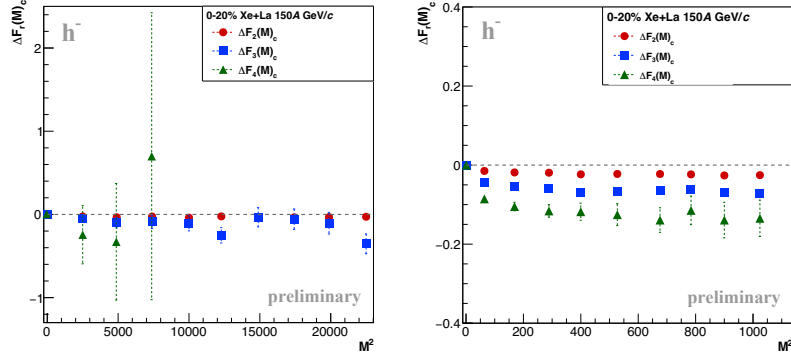


**Figure 14:** Preliminary NA61/SHINE results on the dependence of the scaled factorial moments  $\Delta F_r(M)_c$  ( $r = 2, 3, 4$ ) of multiplicity distributions of negatively charged hadrons on the number of subdivisions in cumulative transverse momentum space  $M^2$  for  $1^2 \leq M^2 \leq 150^2$  (left) and  $1^2 \leq M^2 \leq 32^2$  (right).

### 5.1.10 (OD, OF) Preliminary results on $\pi^-$ , $K^+$ , and $K^-$ production in 0–10% central Xe+La collisions at 30A, 40A, and 75A GeV/c

The new preliminary results (0–10% central Xe+La at 30A, 40A, and 75A GeV/c) were presented for the first time in Refs. [29,31,44,67,68] together with older preliminary results (0–20% central Xe+La at 150A GeV/c) already shown in Refs. [69,70]. The  $\pi^-$  spectra were obtained from the  $h^-$  method [71], where negatively charged pions are computed from negatively charged hadrons and the remaining contribution from other particles is corrected for using Monte Carlo data. The spectra of  $K^+$  and  $K^-$  were obtained from  $dE/dx$  fits. The example rapidity spectra are presented in Fig. 15.

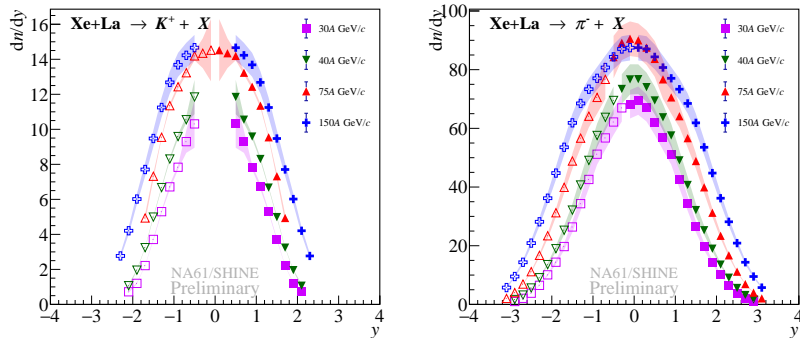


**Figure 15:** Preliminary NA61/SHINE results on rapidity spectra of  $K^+$  measured using  $dE/dx$  method (left) and  $\pi^-$  measured using  $h^-$  method (right) in central Xe+La collisions at 30A, 40A, 75A, and 150A GeV/c. Color bands represent systematic uncertainties, statistical uncertainties do not exceed marker size.

The results on the energy dependence of the  $K^+/\pi^+$  particle yield ratio at mid-rapidity and  $\langle K^+ \rangle / \langle \pi^+ \rangle$  ratio (*horn plots*) from central Xe+La collisions are shown in Fig. 16 together with measurements in inelastic  $p+p$ , central Be+Be, central Ar+Sc, central Pb+Pb, and central Au+Au collisions. A clear distinction between the two data subsets is visible –  $p+p$  and Be+Be results show similar values and collision energy dependence, while the heavy systems of Xe+La, Pb+Pb, Au+Au, and Ar+Sc show much higher  $K^+/\pi^+$  ratios. For Xe+La collisions presented in Fig. 16 the  $\pi^+$  yields were estimated from  $\pi^-$  yields using correction factor calculated from EPOS1.99 as the ratio of  $\langle \pi^+ \rangle_{\text{EPOS}}$  to  $\langle \pi^- \rangle_{\text{EPOS}}$ .

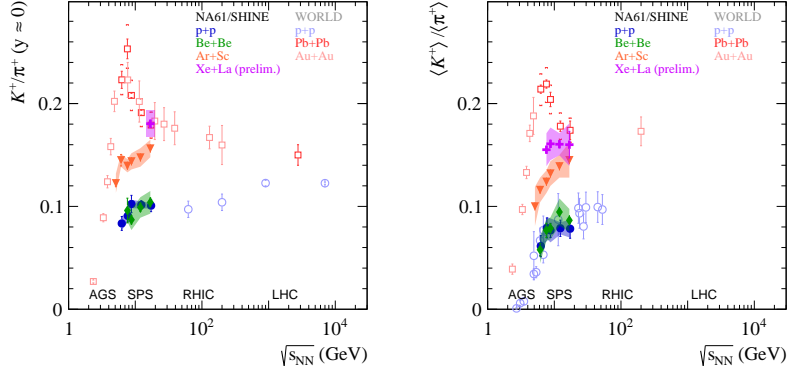


**Figure 16:** The energy dependence of the  $K^+/\pi^+$  particle yield ratio at mid-rapidity (*left*) and  $\langle K^+ \rangle / \langle \pi^+ \rangle$  ratio (*right*) for  $p+p$  and nucleus-nucleus collisions. The NA61/SHINE Xe+La results are preliminary. See Ref. [11] for references to the NA61/SHINE and world data points. For NA61/SHINE data, color bands represent systematic uncertainties and error bars correspond to statistical ones.

### 5.1.11 (OD, O) Preliminary results on $D^0 + \bar{D}^0$ production in 0–20% central Xe+La collisions at 150A GeV/c

This year NA61/SHINE released the preliminary result on the first direct measurement of open charm production in heavy-ion collisions at the SPS energies. The precision of the result allows to disentangle between theoretical models (see below). The preliminary results were presented in Refs. [31,44,72–74].

The analysis was performed on 150A GeV/c Xe+La data recorded in 2017 with the Small Acceptance Vertex Detector (SAVD) installed. The SAVD tracks matched to TPC tracks were used to search for the  $D^0 + \bar{D}^0$  signal. In the analysis presented here, the PID information was not used. Each SAVD track was paired with another SAVD track and was assumed to be either a kaon or a pion. Thus each pair contributes twice to the combinatorial invariant mass distribution. More details about SAVD and open charm reconstruction can be found in Refs. [75,76]. Figure 17 shows the invariant mass distribution of unlike charge daughter candidates with the applied [72] cuts. The peak corresponding to  $D^0 + \bar{D}^0$  has the significance  $\frac{S}{\sqrt{S+B}}$  on the level of  $6\sigma$ .

In order to obtain the corrections and calculate the absolute value of  $D^0 + \bar{D}^0$  yield, the GEANT4 simulations were performed. The background in the MC events was described using the EPOS model, while the signal phase space was parametrized using three models: AMPT, PHSD, and PYTHIA/Angantyr, which predict quite different phase space distribution of open charm.

After applying corrections from MC, the corrected yield for each phase space assumption was calculated. The results are presented in Table 1. The visible yield  $N(D^0 + \bar{D}^0)_{\text{visible}}$  corresponds to the yield in the  $-0.5 < y < 1.0$  and  $0.2 < p_T < 2.0$  GeV/c rapidity-transverse momentum bin covering



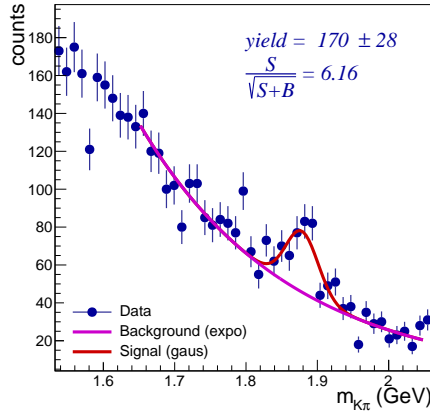


**Figure 17:** The invariant mass distribution of unlike charge sign  $\pi, K$  decay track candidates for Xe+La collisions at 150A GeV/c. The exponential function was used to fit the background, and the Gaussian one was used to describe the  $D^0 + \bar{D}^0$  signal. The indicated errors are statistical only.

correction with:	$N(D^0 + \bar{D}^0)_{\text{visible}}$	$\frac{dN(D^0 + \bar{D}^0)}{dy}_{-0.5 < y < 1.0}$	$\langle D^0 + \bar{D}^0 \rangle$
AMPT	$0.184 \pm 0.032$	$0.129 \pm 0.023 \pm 0.035$	$0.218 \pm 0.039 \pm 0.060$
PHSD	$0.204 \pm 0.036$	$0.148 \pm 0.026 \pm 0.036$	$0.303 \pm 0.054 \pm 0.074$
PYTHIA/Angantyr	$0.201 \pm 0.035$	$0.147 \pm 0.026 \pm 0.037$	$0.300 \pm 0.052 \pm 0.075$

**Table 1:** Preliminary NA61/SHINE results on the visible yield,  $dN/dy$  at mid-rapidity and yield in  $4\pi$  of  $D^0 + \bar{D}^0$  mesons obtained assuming the phase space distribution from AMPT, PHSD, and PYTHIA/Angantyr models. The first indicated uncertainty is the statistical one, and the second is systematic; the visible yields are shown with statistical uncertainties only. The systematic uncertainty does not include the correction to model-dependent phase space.

SAVD acceptance. In order to obtain the  $\frac{dN(D^0 + \bar{D}^0)}{dy}_{-0.5 < y < 1.0}$  and  $4\pi$ -yield  $\langle D^0 + \bar{D}^0 \rangle$  the extrapolation factors for each model were obtained. The AMPT model predicts that about 84% of  $D^0 + \bar{D}^0$  would be in the SAVD acceptance, while PHSD and PYTHIA/Angantyr predict the level of 67%. Thus,  $\langle D^0 + \bar{D}^0 \rangle$  differ significantly between model assumptions.

Figure 18 shows the comparison of the obtained  $4\pi$  yield  $\langle D^0 + \bar{D}^0 \rangle$  to the theoretical model predictions. The precision of the data is sufficient enough to discriminate between model predictions. While microscopic models (AMPT, PYTHIA/Angantyr, PHSD, HSD) tend to significantly underestimate  $D^0 + \bar{D}^0$  yield, ALCOR and SMES models are overestimating it. The obtained result is higher than the scaled proton-nucleus data.

### 5.1.12 (OD, O) Performance results on invariant mass spectra in Pb+Pb collisions taken in 2022

The performance results are based on the Pb+Pb collisions at beam momentum of 150A GeV/c recorded in 2022 since it is currently the most thoroughly investigated data set taken after the LS2. The Vertex Detector (VD) tracks matched to TPC tracks are used to search for the  $D^0 + \bar{D}^0$  signal. The particle

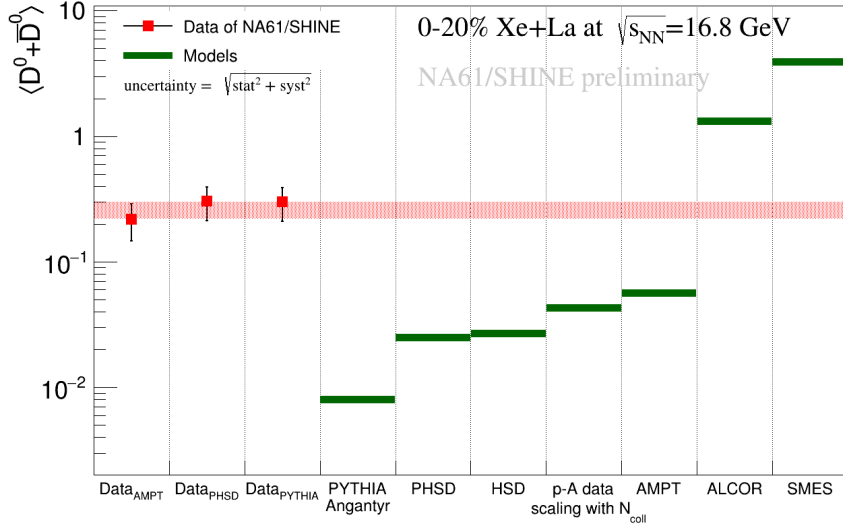


**Figure 18:** Comparison of the obtained NA61/SHINE preliminary result to theoretical model predictions. The red band indicates the theoretical uncertainty of the result due to the unknown phase space distribution of  $D^0, \bar{D}^0$ .

identification (PID) information was not used in the analysis. Each VD track is paired with another VD track and is assumed to be either a kaon or a pion. Thus each pair contributes twice in the combinatorial invariant mass distribution. The combinatorial background is several orders of magnitude higher than the  $D^0 + \bar{D}^0$  signal due to the low yield of charm particles. Five cuts were applied to reduce the large background. The cut parameters were chosen to maximize the signal-to-noise ratio (SNR) of the reconstructed  $D^0 + \bar{D}^0$  peak and were determined from the GEANT4-based Monte Carlo simulations. These cuts are:

- (i) cut on the track transverse momentum,  $p_T > 0.32 \text{ GeV}/c$ ;
- (ii) cut on the track impact parameter,  $d > 50 \text{ }\mu\text{m}$ ;
- (iii) cut on the longitudinal distance between the  $D^0$  decay vertex candidate and the primary vertex,  $V_z > 1450 \text{ }\mu\text{m}$ ;
- (iv) cut on the impact parameter  $D$  of the back extrapolated  $D^0$  candidate momentum vector,  $D < 32 \text{ }\mu\text{m}$ ;
- (v) cut on daughter tracks distance at the closest proximity,  $DCA < 50 \text{ }\mu\text{m}$ .

The  $d$  and  $D$  parameters are defined as the shortest distance between the primary vertex and the track line of a single track and  $D^0$  candidate, respectively. Note that the last four cuts are based on information delivered by the VD.

Figure. 19 shows the invariant mass distribution of unlike charge daughter candidates with the applied cuts for events with VD tracks multiplicity smaller than 350. The above-mentioned selection was used due to the efficiency of the TPC tracking algorithm for central Pb+Pb collisions. One observes a peak emerging at 1.86 GeV, consistent with a  $D^0 + \bar{D}^0$  production. The invariant mass distribution was fitted using an exponential function to describe the background and a Gaussian to describe the  $D^0 + \bar{D}^0$  signal contribution. The line representing the signal plus the background is

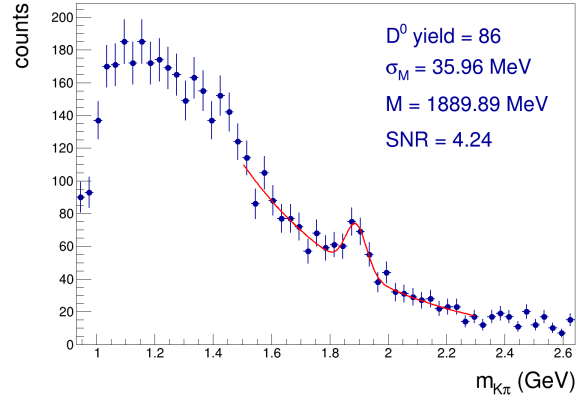


**Figure 19:** The invariant mass distribution of unlike charge sign  $\pi, K$  decay track candidates for Pb+Pb collisions at  $150A$  GeV/c taken in 2022. The presented results refer to 5M events of Pb+Pb interactions at the most downstream 1 mm layer of the target.

drawn in red on the plot. The indicated uncertainties are statistical only. The total yield amounts to  $86 \pm 28$  with a  $\pm 3\sigma$  integrated SNR of 4.24.

An intense effort is currently put into improving the quality of track reconstruction, namely:

- (i) improvement of TPC tracking efficiency;
- (ii) tuning TPC chambers relative geometry;
- (iii) improvement of VD sensor inner geometry;
- (iv) tuning of global VD and TPC geometry.

These improvements should lead to a significant increase of reconstructed  $D^0 + \bar{D}^0$  signal. The estimates from the simulations indicate that, on average, about 200  $D^0 + \bar{D}^0$  will be reconstructed per one million of the collected minimum bias events. The Collaboration intends to obtain the results within a few weeks.

### 5.1.13 (O) Preliminary results on $\phi$ meson production in 0–10% central Ar+Sc collisions at 40A, 75A, and 150A GeV/c

The preliminary results on  $\phi(1020)$  meson production in central Ar+Sc collisions at three beam momenta (40A, 75A, and 150A GeV/c) were obtained and presented in Refs. [77–79]. To extract the  $\phi$  yields, the invariant mass spectra were constructed from pairs of  $K^+$  and  $K^-$  candidates, as this is the main (around 50%) decay channel of  $\phi$ .

Further, the tag-and-probe method [80] was applied to the invariant mass spectra to extract the uncorrected  $\phi$  meson yields in selected  $(y, p_T)$  bins. The final  $d^2n/dydp_T$  spectra are corrected for detector effects (based on MC simulations) and branching ratio. The rapidity spectra  $dn/dy$  are obtained from the corresponding  $p_T$ -extrapolated and integrated  $d^2n/dydp_T$  distributions. The mean multiplicities of  $\phi$  mesons  $\langle\phi\rangle$  are then computed from integrated rapidity distributions.

The left panel of Fig. 20 shows the ratio of  $\phi$  yield to the  $\pi$  yield as a function of the collision energy for  $p+p$ , Ar+Sc, and Pb+Pb reactions. This ratio increases with energy, and data points from Ar+Sc are higher than for  $p+p$ , and almost as high as for Pb+Pb collisions. The middle panel presents the double ratios, which are the yield ratios of  $\phi$  to  $\pi$ ,  $K^+$  to  $\pi^+$ , and  $K^-$  to  $\pi^-$  from Pb+Pb divided by

the corresponding ratios from  $p+p$ . For the highest collision energy, the ratio of  $\phi$  over  $\pi$  is higher than for  $K^+/\pi^+$  and  $K^-/\pi^-$ . The right panel shows the same double ratios as above but for Ar+Sc instead of Pb+Pb reactions. The  $\phi$  over  $\pi$  ratio is typically higher than  $K^+/\pi^+$  and  $K^-/\pi^-$ .

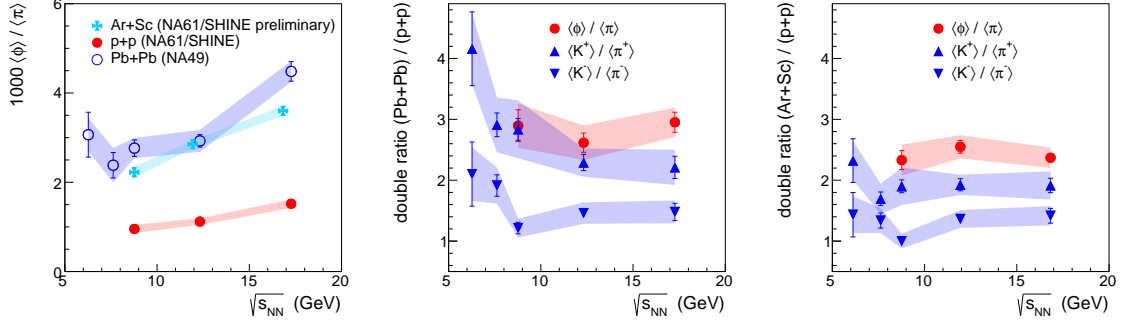


**Figure 20:** *Left:* The ratio of  $\phi$  yield to  $\pi$  yield as a function of collision energy for  $p+p$ , Ar+Sc, and Pb+Pb. *Middle:* The double ratios – the yield ratios of  $\phi$  to  $\pi$ ,  $K^+$  to  $\pi^+$ , and  $K^-$  to  $\pi^-$  from Pb+Pb divided by the corresponding ratios from  $p+p$ . *Right:* The same as *middle* but Ar+Sc instead of Pb+Pb. The  $\phi$  multiplicities in Ar+Sc are NA61/SHINE preliminary, the  $\phi$  yields in NA61/SHINE  $p+p$  and NA49 Pb+Pb are taken from Refs. [80,81], and the kaon and pion data in  $p+p$ , Ar+Sc, and Pb+Pb are taken from Refs. [11,56,58,82].

## 5.2 New results for neutrino physics

The NA61/SHINE Collaboration continues to execute its program of hadron production measurements for long-baseline neutrino oscillation experiments at J-PARC and Fermilab (FNAL). These measurements allow for an improved knowledge of the neutrino fluxes produced in accelerator-based neutrino beams. NA61/SHINE measures total cross-sections and differential spectra of hadron yields from thin and replica neutrino beam targets. The Run 2 data sets were aimed primarily at measurements relevant for the FNAL long-baseline neutrino program, which uses 120 GeV/ $c$  protons in both its current (NuMI/NOvA) and planned next-generation (LBNF/DUNE) beams. Progress continues in publishing full double-differential spectrum results from these data sets, with a new paper on 90 GeV/ $c$   $p+C$  interactions submitted this year following two papers on 120 GeV/ $c$   $p+C$  [83,84] that were published last year. Additionally, analysis is in progress on the first Run 3 physics data set, a high-statistics 2022 run with 31 GeV/ $c$  protons on a new replica target for the T2K experiment.

### 5.2.1 Yields of charged and neutral hadrons from $p+C$ at 90 GeV/ $c$ interactions (FNAL)

The yields of neutral and charged hadrons from 90 GeV/ $c$  proton-carbon interactions were measured from a dataset taken by the NA61/SHINE experiment in 2017. While the primary interaction for long-baseline neutrino beams at Fermilab is between a 120 GeV/ $c$  proton and a carbon nucleus, secondary and tertiary interactions occurring inside and outside the target volume contribute significantly to the neutrino beam flux [85]. Measuring hadronic production for these secondary and tertiary interactions, like 90 GeV/ $c$  proton-carbon interactions, will enable more accurate predictions of the neutrino beam flux by providing additional points to constrain interaction models.

Yields of charged hadrons  $\pi^\pm$ ,  $K^\pm$ , and  $p/\bar{p}$  were found by a fit to the  $dE/dx$  distribution in each kinematic bin; Fig. 21 shows sample multiplicities for  $\pi^\pm$ . The neutral hadrons  $K_S^0$ ,  $\Lambda$ , and  $\bar{\Lambda}$  were identified via an invariant mass analysis of their decays to charged hadrons; a sample of these fits

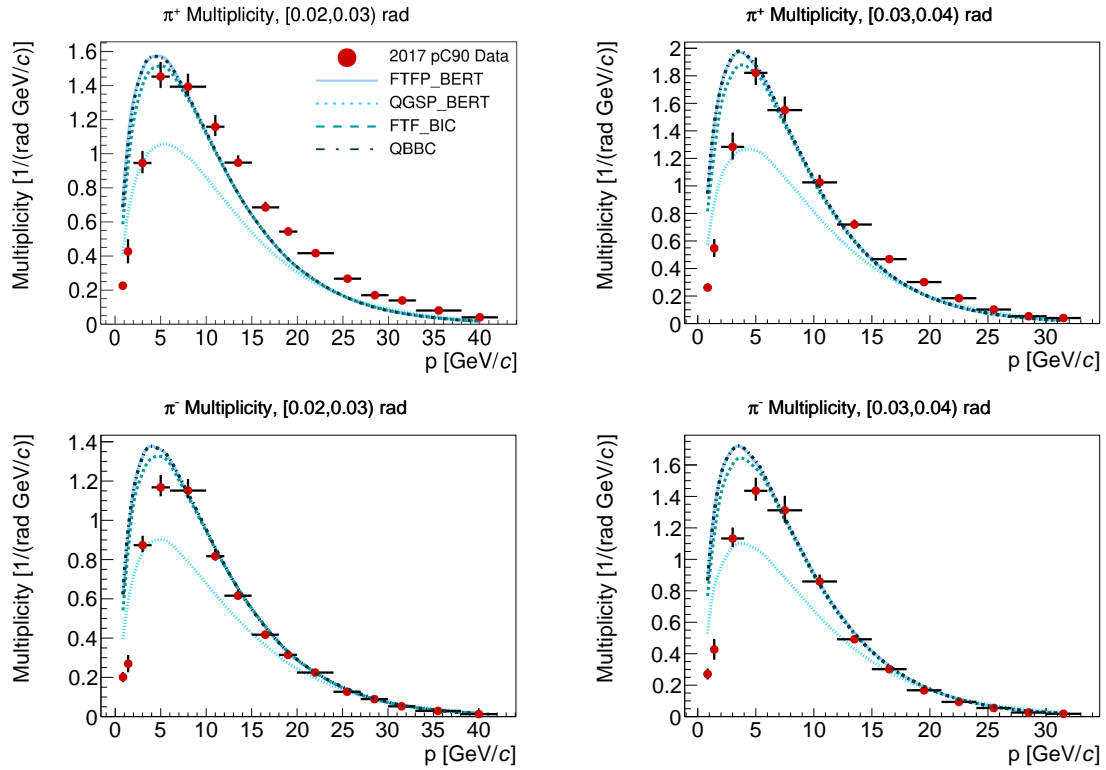


**Figure 21:** Example  $\pi^\pm$  multiplicity measurements from 90 GeV/c proton-carbon interactions for the angular bins [0.02, 0.03] rad and [0.03, 0.04] rad. The uncertainties shown are the total uncertainty. The data points, shown in red, are compared to four physics lists from GEANT4 version 10.7.0. Figure from Ref. [87].

is shown in Fig. 22. Double-differential multiplicity spectra as a function of laboratory momentum were obtained for each particle species in polar angle bins ranging from 0 to as high as 350 mr.

The final measured multiplicities, including the individual contributions of the systematic uncertainties along with covariance matrices, are available at [86]. A manuscript has been submitted for publication in Phys. Rev. D [87].

## 5.2.2 Neutrino analyses in progress

**$p+C$  at 60 GeV/c (FNAL):** As with  $p+C$  interactions at 90 GeV/c, the 60 GeV/c data set collected in 2016 is intended to constrain models of secondary hadronic interactions in neutrino beams. The analysis is well advanced. The differential yields of neutral particles ( $K_S^0$ ,  $\Lambda$ ,  $\bar{\Lambda}$ ) were obtained using both Native SHINE and Wrapped Legacy reconstructions. The high background-signal ratio of the  $V^0$  candidates in the Native SHINE case indicates continuing issues with the native reconstruction chain, which has only been used for single charged-particle analyses so far. Work is ongoing to understand the effect of tuning local track merging on  $V^0$  selection with the goal of using the native SHINE reconstruction for a  $V^0$  physics analysis for the first time. The dE/dx calibration of the 2016  $p+C$  at 60 GeV/c data has been re-done using the Native SHINE Framework for the charged particle analysis. The central values of differential yields of charged particles ( $\pi^\pm$ ,  $K^\pm$ ,  $p$ ,  $\bar{p}$ ) have been obtained. Cross-checks with multiplicity measurements from 31 GeV/c, 90 GeV/c, and 120 GeV/c

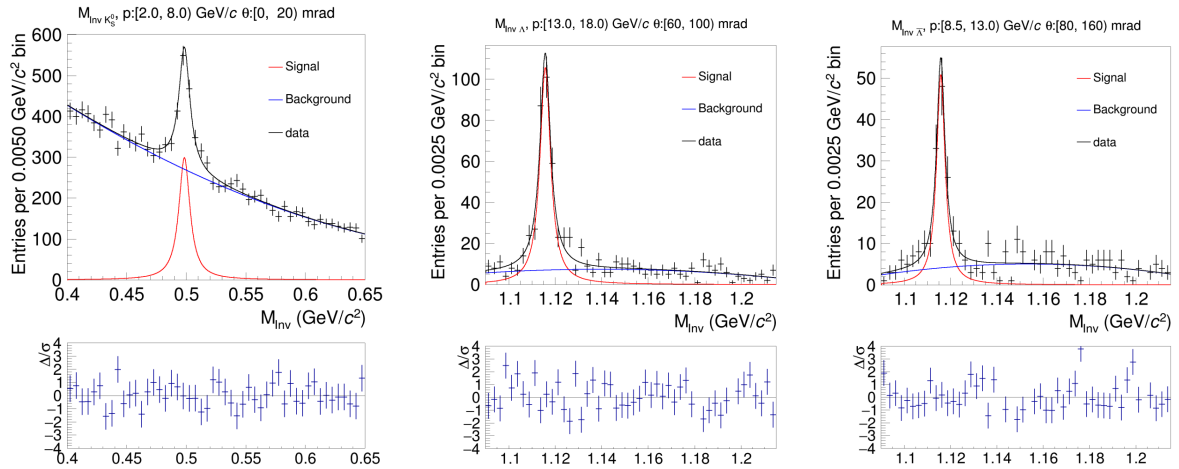


**Figure 22:** Example invariant mass fits for  $K_S^0$ ,  $\Lambda$ , and  $\bar{\Lambda}$  in the 90 GeV/c  $p + C$  analysis. The signal shape is shown alone in red, the background is shown in blue, and the sum of the signal and background is shown in black. At the bottom of each fit is a plot of the fit residual over the statistical uncertainty on the number of entries for each bin; the fit residual is the fit result minus the number of entries. Figure from Ref. [87].

proton-carbon interactions are in progress; systematic uncertainties will be evaluated following the cross-checking.

**$p + \text{NOvA}$  target at 120 GeV/c (FNAL):** The  $p + \text{NOvA}$  target data set from 2018 is nearing the final steps of calibration. The positions of beamline components were determined from data in previous years' work. This year, drift velocity in the TPCs was calibrated for the 2018 data set. This allows precise momentum measurements that are a direct observable of the envisioned charged particle multiplicity result and critical to particle selection for a neutral multiplicity result. The TPCs are currently being calibrated for  $dE/dx$  reconstruction which is the last requirement for the neutral multiplicity analysis. Analysis software has been tested on a Monte Carlo sample and is ready for data. Phase space acceptance observed in the analysis of neutral particle Monte Carlo roughly matches that for NA61/SHINE's T2K replica target neutral multiplicity result.

**$p + \text{T2K}$  target at 31 GeV/c (J-PARC):** NA61/SHINE's first physics data set after Long Shutdown 2 was a high-statistics study of particle production with 31 GeV/c protons on a replica target for the T2K experiment. The detector recorded  $1.8 \times 10^8$  events in summer 2022, nearly a factor of twenty higher than the previous replica T2K target data set in 2010 which reduced T2K's flux errors to the 5% range in the flux peak. The motivation for the new data set is the remaining uncertainty on high-momentum kaon production, which is a systematic error in the "wrong-sign"<sup>1</sup> neutrino background to  $CP$ -violation searches at T2K.

The analysis of the  $p + \text{T2K}$  target data collected in summer 2022 requires the calibration of the TPCs post-LS2. In particular, some chambers have been moved during the upgrade of the detector and it was found that a bias in the assumed position of the chamber deteriorates the drift velocity calibration. A precise calibration of the chambers position after LS2, using field-off data, is ongoing.

<sup>1</sup> A wrong-sign neutrino in a beam is an antineutrino produced in the neutrino beam configuration, or vice-versa.

For neutral kaon analysis, checking the difference between  $K_S^0$  and  $K_L^0$  production is ongoing. This is necessary to input the NA61/SHINE result to T2K beam simulation. Target z-binning study for neutral kaon is also ongoing. Binning into five sections is used for charged hadrons' analyses, but binning for neutral hadrons should be considered separately.

As for the analysis of charged kaons, the study of track acceptance is ongoing. This study is needed to reject tracks with poor acceptance because track analysis performance depends on detector acceptance. It is studied by comparing the true tracks and reconstructed tracks of Monte Carlo samples. The result of the calculation will be used in the cut for raw data analysis to reduce the model dependence of the particle yields.

A final challenge in this analysis is the use of a unique GEM-based temporary beam position detector (BPD) system for this data set, which necessitated the (now complete) development of a new BPD reconstruction and calibration algorithm.

## 5.3 New results for cosmic-ray physics

### 5.3.1 Production of Anti-Nuclei in the Galaxy

Detecting cosmic anti-nuclei can be a breakthrough approach for identifying dark matter [88]. The primary source of cosmic anti-nuclei background are interactions between cosmic-ray protons and interstellar hydrogen gas [89]. Gaining a deeper insight into deuteron production in  $p+p$  interactions is an essential first step in modeling these astrophysical processes [90,91]. The two most prevalent formation models, the thermal and coalescence models, are based on different underlying physics. A better understanding of (anti)nuclei production mechanisms is needed, which drives the effort to analyze high-statistics data sets from fixed-target experiments [91].

#### Proton and antiproton production measurements in $p+p$ collisions at 158 GeV/c

The charged-hadron analysis is based on the combined high-statistics 158 GeV/c  $p+p$  data sets collected in 2009, 2010, and 2011 with a total of about 65 M events. The preliminary transverse momentum particle spectra [92] in rapidity slices for protons and antiprotons were updated. The proton spectra were extended to  $y_{\text{CM}} = 2.3$ . This was done by extending the proton identification region beyond  $p_{\text{lab}}=100$  GeV/c to include the identified proton contributions up to  $p_{\text{lab}}=150$  GeV/c. The antiproton spectra were extended to  $y_{\text{CM}} = 2.1$ . Fig. 23 shows the updated spectra as well as comparisons with the EPOS-LHC model [93].

#### Deuteron production measurements in $p+p$ collisions at 158 GeV/c

Deuteron production is rare in  $p+p$  interactions at SPS energies of about 100–400 GeV. For  $p_{\text{beam}} = 158$  GeV/c, the coalescence parametrization developed in Refs. [90,91] predicted a per-event production probability of 0.0004, with an uncertainty band from 0.0002–0.0009. Using these estimates, about 10,000–60,000 deuterons are expected to have been produced in the high-statistics  $p+p$  data. However, because of the limited phase space acceptance of the ToF detectors, only a fraction of the total deuterons produced can be identified. The deuteron rapidity region accessible to the ToF detectors coincides with peak deuteron production in the center-of-mass frame's backward hemisphere [91].

The standard ToF- $dE/dx$  analysis technique relies on two-dimensional fits performed in the  $m^2$ - $dE/dx$  plane and was successful in identifying charged hadrons in  $p+p$  and Ar+Sc data sets [11,56]. However, this technique is unable to estimate the deuterons under the proton tail. Therefore, a new data-driven template fitting method was developed for particle identification [94]. For each ( $p$ ,  $p_T$ ) bin, pions and positrons were separated from the other particles using the  $dE/dx$  information. As the mass distributions for kaons, protons, and deuterons overlap, the pion mass distribution was



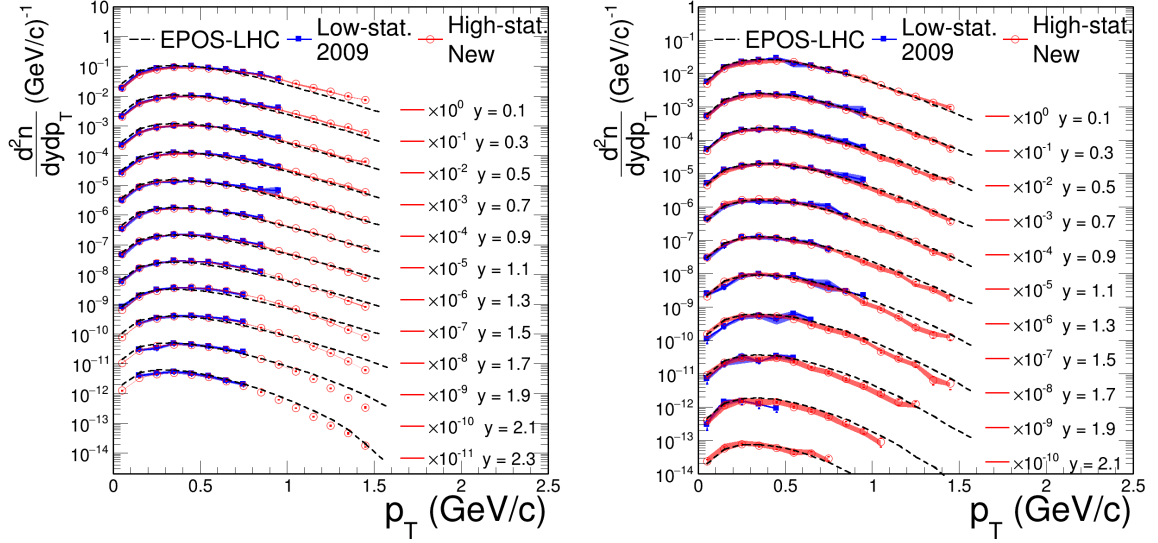


**Figure 23:** Transverse momentum particle spectra in rapidity slices for protons (left) and antiprotons (right) produced in inelastic  $p+p$  interactions at 158 GeV. The updated preliminary results from the combined high-statistics  $p+p$  data set at 158 GeV/c are shown in red, and the previously-published results in Ref. [56], from the analysis of the 2009  $p+p$  data set are shown in blue. Shaded bands show systematic uncertainties. Dotted black lines show the comparisons with the EPOS-LHC model [93].

modified for detector resolution effects and the kaon, proton, and deuteron mass, respectively. These three modified mass templates served as the input for the combined one-dimensional  $m^2$  template fit of the higher-mass  $Z = 1$ -particle mass spectra. Fig. 24 (left) shows an example  $(p, p_T)$  bin with a clear deuteron peak. It also illustrates the importance of realistically estimating the proton tail in the deuteron mass region. The kaon, proton, and deuteron yield extraction is based on the probability method already developed for the  $dE/dx$ -only analysis. To finalize the particle spectra, the correction factors for detector geometry and ToF-related efficiencies were calculated using Monte Carlo simulations.

The new technique was validated in two independent ways. First, in each  $(p, p_T)$  bin, the fitted proton counts from the new technique were compared to the fitted proton counts from the standard method. This ratio was found to be exactly 1 in almost all  $(p, p_T)$  bins, with a very small associated uncertainty. Next, the identified proton spectra from the new ToF- $dE/dx$  technique was compared to the identified proton spectra from the  $dE/dx$ -only analysis (Fig. 23 (left)) for the available overlapping phase space bins. This comparison is shown in Fig. 24 (right). Both spectra overlap within the uncertainty bands, which validates the new technique.

Fig. 25 (left) shows the transverse momentum spectra in rapidity slices for deuterons produced in inelastic  $p+p$  interactions at 158 GeV. An overlay of the thermal model (solid lines) is also shown. The thermal model is characterized by two parameters: the temperature  $T$ , which defines the shape of the distribution, and an amplitude factor. For illustrative purposes, the temperature has been set to  $T = 150$  MeV (from [56]), and only the amplitude has been fitted to the data. The thermal model overlay demonstrates the agreement between the data and the thermal model at this initial stage of the analysis.

Detailed cross-checks have been developed to account for the deuterons produced by secondary protons in the target material or holder. The contribution of secondary proton interactions with the right

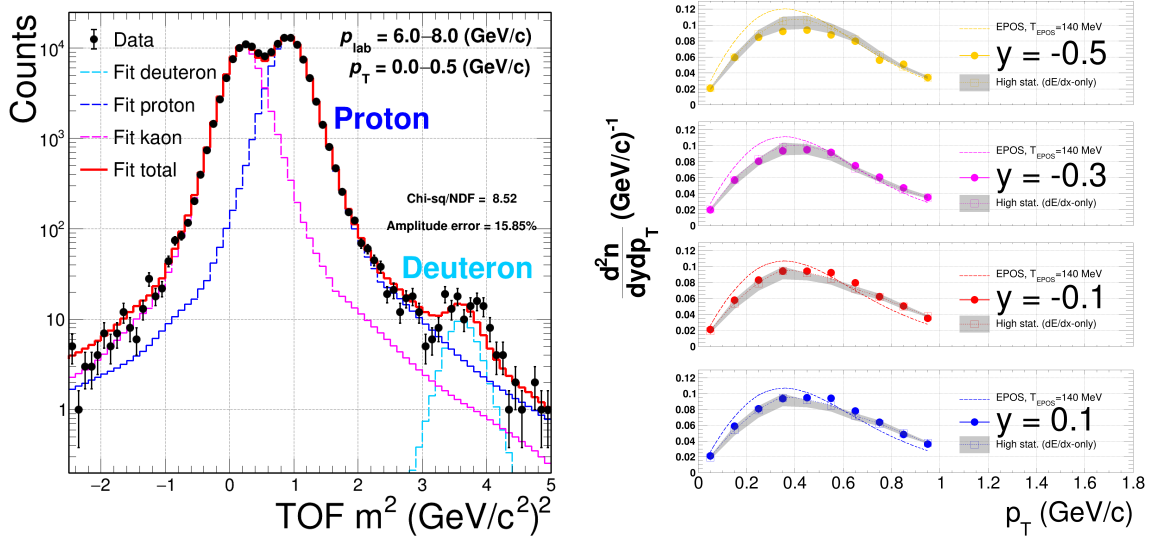


**Figure 24: Left:** Data-driven pion mass template fits were used to fit the kaon, proton, and deuteron peaks and tail regions, shown here for an example phase space bin. Data and fitted protons, kaons, and deuterons are shown. A clear deuteron signal is visible. Correctly estimating the proton tail under the deuteron signal is of critical importance. **Right:** Comparison of the identified proton transverse momentum spectra in rapidity slices from the new technique versus the identified proton spectra from the  $dE/dx$ -only analysis (Fig. 23 (left)). The two spectra overlap within the uncertainty bands. The dotted lines show the comparisons with the EPOS-LHC model [93] for illustration.

target holder was estimated to be negligible. The contribution of secondary protons re-interactions within the liquid hydrogen of the target was estimated to be less than  $\sim 2\%$  [91]. Further studies to estimate the secondary deuteron background using Geant4 simulation are ongoing. Next, systematic and statistical uncertainties will be estimated. The dominant sources of systematic uncertainties are those associated with the one-dimensional  $m^2$  fits and the modeling of the proton tail under the deuteron peak. The preliminary release of these results will follow.

### Two-proton femtoscopy measurements in $p+p$ collisions at 158 GeV/c

Two-proton correlation studies have been measured at high energies (e.g., ALICE [95]), but no accepted theory exists to predict the source size at low energies. NA61/SHINE has conducted correlation studies before, but either without particle identification [96, 97] or for pions [37], which are easier to identify than protons. The 158 GeV/c  $p+p$  data enable determining the source size from proton pairs in this energy range for the first time, making it a crucial result to complement RHIC and ALICE measurements at high energies. The right panel of Fig. 25 demonstrates the initial  $C(k^*)$  measurement status. Proton pairs were extracted from the data, ensuring that protons from detector interactions and  $\Lambda$  decays are suppressed to a minimum. The result shows a clear difference from a uniform distribution, and a provisional correlation function fit suggests a source size of 1–2 fm.

However, the statistics are low, and only about 180 proton-proton pairs have been identified in the low  $k^*$  region. Increasing the number of identified proton pairs is essential to reduce the statistical uncertainties currently dominating the extracted source size. Efforts to improve the proton-pair statistics and the fit quality are ongoing. Monte Carlo corrections for detector effects will be estimated next. Estimation of systematic uncertainties will follow after that.

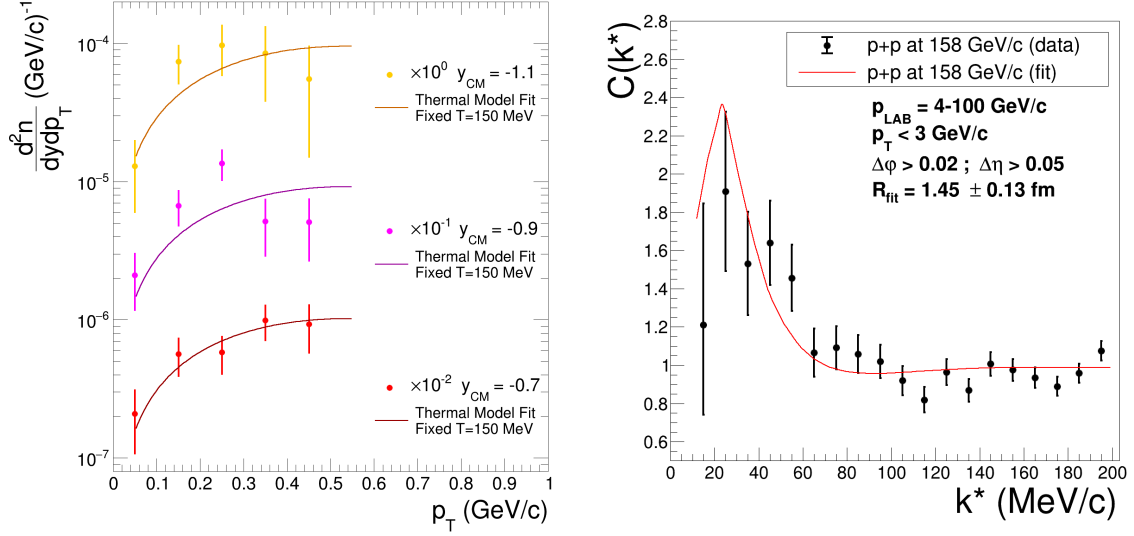


**Figure 25: Left:** Work-in-progress transverse momentum spectra in rapidity slices for deuterons produced in inelastic  $p+p$  interactions at 158 GeV. Solid lines show the overlaid two-parameter thermal model with the shape parameter set to  $T = 150$  MeV (from [56]) prior to the fit. Only the amplitude parameter was fitted to the data. **Right:** Work-in-progress  $p-p$  correlation function as a function of  $k^*$ , the relative momentum of the proton pair in the pair center-of-mass frame, for the high-statistics  $p+p$  158 GeV/ $c$  data set (black points) along with the best-fit line in red.

The ultimate goal of measuring the interaction source size and the antiproton differential production cross section is to construct a data-driven (anti)deuteron coalescence model. The model will be validated by comparing its predictions with the measured deuteron yield from the same data set. The 158 GeV/ $c$  data provides the first proof that a model for (anti)deuteron production can be constructed using such measurements.

### 5.3.2 Fragmentation of Cosmic-Ray Nuclei in the Galaxy

Cosmic ray (CR) propagation characteristics are currently dominated by the large uncertainties in the nuclear fragmentation cross sections at  $\sim 20 - 30\%$ . While, the precision on recent flux measurements by detectors like AMS-02, CALET and DAMPE are  $< 5\%$ , it is crucial to perform laboratory measurements of the fragmentation cross sections with the same precision, to determine CR transport parameters in the Galaxy. The boron-to-carbon (B/C) flux ratio is the simplest to measure and is the most well-studied secondary-to-primary ratio. Hence, a precise nuclear fragmentation cross-section leading to boron production will aid in studying CR propagation in the Galaxy. In 2018, a pilot run demonstrated the feasibility of performing fragmentation studies with NA61/SHINE. We have derived the boron isotope production ( $^{10}\text{B}$  and  $^{11}\text{B}$ ) in  $^{12}\text{C}+p$  reaction at 13.5A GeV/ $c$  using the polyethylene (PE) and graphite (C) targets. Moreover,  $^{11}\text{C}$  is a radionuclide with a half-life  $\tau_{1/2} \approx 20$  min, which decays to  $^{11}\text{B}$  as  $^{11}\text{C} \rightarrow ^{11}\text{B} + \beta^+ + \nu_e$ , and contributes to the total boron production in the Galaxy. Therefore, we also calculated the  $^{11}\text{C}$  production cross section from the pilot data.

A combined log-likelihood fit is performed to the fragment distribution in the MTPC, for the three target settings, namely, PE, C, and OUT to determine the isotope yields. The fit results to the boron

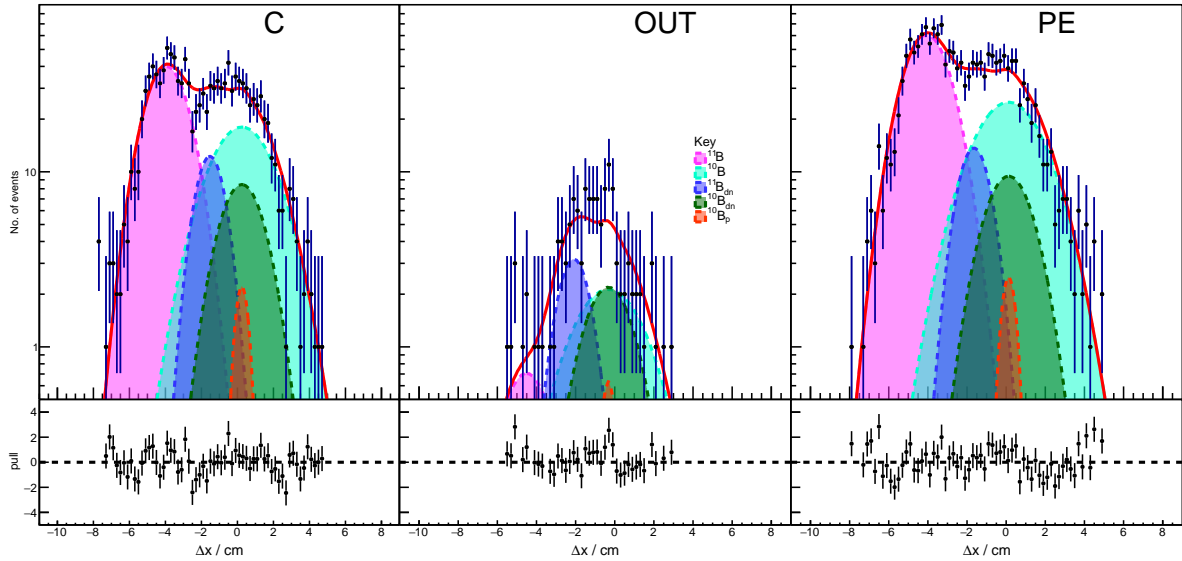


**Figure 26:** A combined fit result to the boron fragment distribution as measured in the MTPC. The *teal* and *pink* peaks correspond to the  $^{10}\text{B}$  and  $^{11}\text{B}$  fragments produced at the target. Whereas the *green* and *blue* peaks are the  $^{10}\text{B}$  and  $^{11}\text{B}$  produced downstream of the target, inside the magnetic field of the VTTCs. The narrow *orange* peak corresponds to the  $^{10}\text{B}$  present in the beam composition.

fragment distribution are shown in Fig. 26. The production cross-sections of carbon and boron isotopes were measured and presented at the 37<sup>th</sup> and the 38<sup>th</sup> International Cosmic Ray Conferences, respectively. Our results of the production of  $^{11}\text{C}$ ,  $^{11}\text{B}$ , and  $^{10}\text{B}$  are in good agreement with previous measurements and the various cross section parameterization model lines, shown in Fig. 27. It is interesting to note that apart from our result, there are no direct boron production measurements at momentum  $p > 10A \text{ GeV}/c$ . A publication summarizing the boron production measurement based on the pilot run has been submitted to PRC [98].

The measurements from the pilot run are dominated by statistical uncertainties. More precise data is expected to be collected during the high-statistics fragmentation run scheduled in November 2024. This run aims to study the fragmentation of primary CR species like C, N, O, and Si, providing measurements on the production of lighter fragments like Be and Li isotopes.

## 6 Beam request for 2025 and 2026 and plans after LS3

Recently, CERN has revised its schedule for its accelerator complex. The Run 3 data-taking period was extended until July 2026 for LHC and until August 2026 for SPS. The third Long Shutdown (LS3) will begin seven and a half months later than originally planned. The HL-LHC (Run 4) start-up is now planned for June 2030. The beginning of the physics at SPS may be expected in 2029 or 2030. The accelerator-schedule revision led to the revision of the NA61/SHINE beam request, presented below.

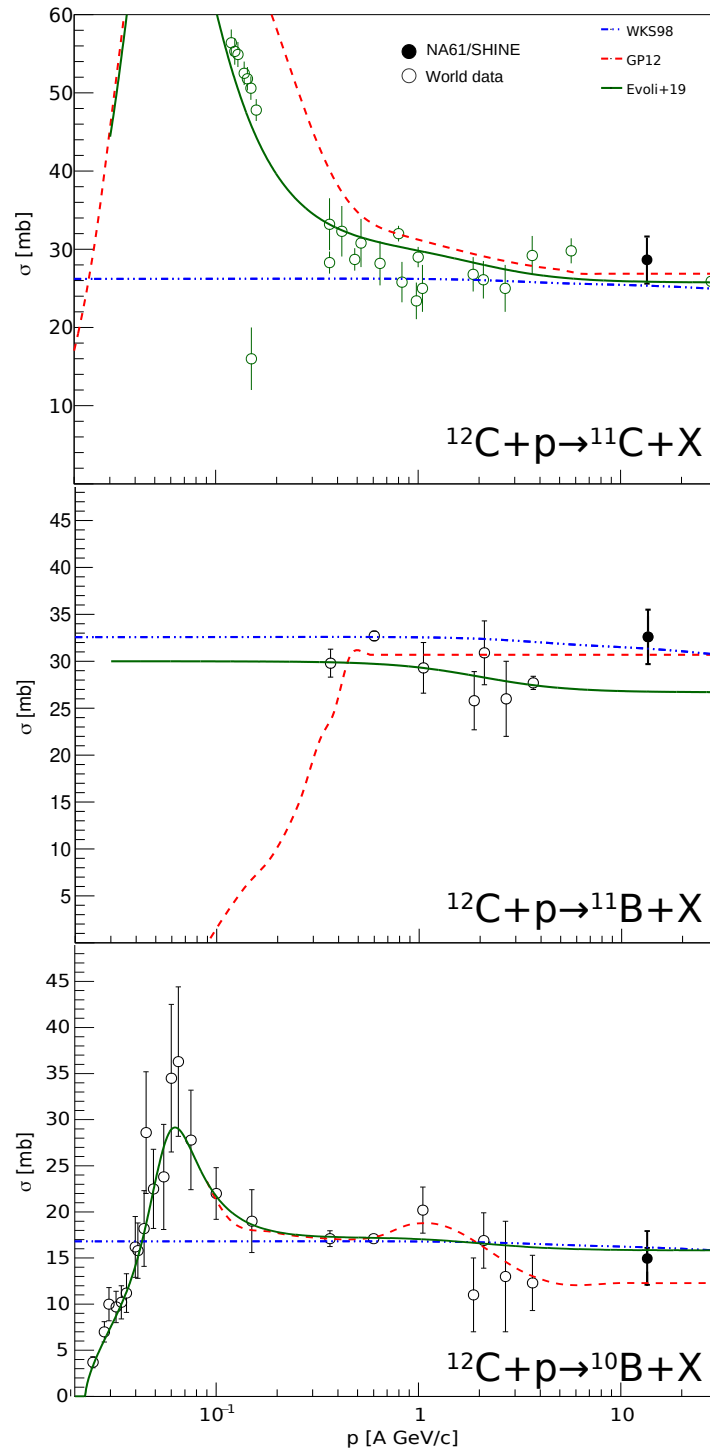


**Figure 27:** Carbon and boron isotope cross section results. The lines correspond to various cross section parameterization models.

## 6.1 Ion beams in 2025 and 2026

The SPS Coordinator organized a meeting with the BE representatives on October 28 to discuss the experiment's physics priorities and the accelerator's chain constraints concerning the data-taking with the ion beams in 2025 and 2026. The following proposal was agreed:

1. 2025: 9 days of O beam at 150A GeV/c for the study of the onset of fireball and charge-symmetry violation,
2. 2025: 2 weeks of Pb beam at 150A GeV/c for open charm production,
3. 2026: 4 weeks of Pb beam at 150A GeV/c for open charm production.

Thus, 7 weeks and 2 days with ion beams are requested. This is the same time as initially planned, 2025: 2 days of O, 2 weeks of Pb and 2026: 4 weeks of Pb. However, it is distributed differently between 2025 and 2026 and between O and Pb beams. The optimized request lets us get the first physics results from O+O collisions at 150A GeV/c well before LS3. Using these results, the post-LS3 light ion programme [99, 100] can be optimized. Moreover, the open charm measurements in Pb+Pb collisions will profit from the extended Pb beam time by 2 weeks.

## 6.2 Hadron beams in 2025 and 2026

NA61/SHINE request four weeks of beam time in 2025 for crucial measurements in high-statistics p+p interactions at 300GeV/c [2] (approximately  $10\times$  larger (600 M events) than the previously analyzed 158A GeV/c dataset):  $p\bar{p}$  correlations, deuteron production cross sections, and the first-ever antideuteron production cross section in this energy range. Additionally, it will be used to measure antiproton production cross-sections with unprecedented precision. Together, these measurements will be instrumental in building and validating a state-of-the-art model for producing astrophysical antideuterons.

For neutrino physics, we request three weeks of data collection in 2025 using 120 GeV/c protons to study interactions on a second LBNF prototype target with identical dimensions but made of a lower-density type of graphite (IG430 instead of IG510). LBNF/DUNE has not settled on a final graphite type, and having data at two different density values will allow interpolation or extrapolation to other density values if needed in the future. (Due to the difference in longitudinal positions of interactions and different containment of secondary particles within the target diameter, density scaling is less straightforward than simulating additional material in the beam or target.)

Neutrino physics beam requests for 2026 will depend on the development of the low-energy beam [101–103]: in the event that the beam is constructed in the 2025-26 YETS, we anticipate requesting 8.9 GeV/c protons on a beryllium target, in order to provide measurements to improve flux estimation for the Booster Neutrino Beam at Fermilab.

## 6.3 Plans after LS3

During the third Long Shutdown of the CERN accelerator complex during 2027-2029, NA61/SHINE plans to perform a major upgrade, allowing to take data in two modes. The upgrade will replace the first large-volume Time Projection Chamber (VTPC-1) with the fast (up to 10k Hz data rate) tracker. It will include high-precision silicon-pixel detectors placed close to the target and larger area gas detectors located downstream. In the first mode of operation, the new tracker will operate together with the existing detectors (TPCs and ToFs), recording data similar to the current NA61/SHINE data with a rate of 1k-2k Hz. The new tracker will operate alone in the second mode, recording data with a 10k Hz rate. The latter will allow us to measure charm-anticharm quark correlations in central Pb+Pb

collisions with a single heavy-quark pair produced per collision. This will provide a unique input constraining the diffusion of charm quarks and verifying assumptions concerning the production locality of a charm and anti-charm quark pair [104].

The upgraded detector will allow us to perform the requested measurements with light ions [99, 100] and continue measurements for neutrino and cosmic-ray physics. Importantly, it will allow for the unique measurements of correlations between charm and anti-charm hadrons in central Pb+Pb collisions at the CERN SPS, where, at most, one heavy quark pair is produced [104].

## 7 Summary

This NA61/SHINE annual report briefly presents the status and plans of the NA61/SHINE experiment [1] at the CERN SPS. The report refers to the period December 2024 – November 2025.

The summary of this report is as follows:

- (I) In October 2024, the NA61/SHINE experiment received a 150A GeV/c Pb beam, data for charm production in Pb+Pb. We gathered 180 million Pb+Pb interactions throughout 2022 and 2023 (see Section 2).
- (II) NA61/SHINE collected data with secondary hadron beams for four weeks in July 2024 with a 150-cm-long LBNF/DUNE prototype target made of IG510 graphite (see Section 2). The initial physics run commenced with settings at half magnetic field (80 GeV/c field) and transitioned to full magnetic field settings (158 GeV/c field) after 10 days. The recorded dataset statistics consist of 124.7 million and 114.3 million proton interactions on the LBNF prototype target, respectively, for the two magnetic field settings.
- (III) The reconstruction and calibration software is continuously maintained and developed (see Section 4). The main activities were to update the offline and online software. The core of the data acquisition (DAQ) system was migrated to the DAQing software framework. The migration initiative came from the CERN EP-DT-DI department. The new calibration software tools were implemented to collect data from the upgraded detector. The calibration procedure for data collected in 2022 and 2023 is advanced, especially for TPCs and Vertex Detector.
- (IV) New physics results, final and preliminary, were released (see Section 5): Results relevant for the NA61/SHINE study of the onsets of deconfinement and fireball and search for the critical point include:
  - (a)  $\pi^\pm, K^\pm, p,$  and  $\bar{p}$  production in 0–10% central Ar+Sc collisions at 13A–150A GeV/c
  - (b)  $K_S^0$  meson production in 0–10% central Ar+Sc collisions at 75A GeV/c
  - (c) higher-order moments of multiplicity and net-electric charge distributions in inelastic  $p+p$  collisions at 20–158 GeV/c
  - (d) proton intermittency in 0–10% central Ar+Sc collisions at 13A–75A GeV/c
  - (e)  $K_S^0$  meson production in inelastic  $p+p$  collisions at 31, 40, and 80 GeV/c
  - (f) femtoscopy analysis in 0–10% central Ar+Sc collisions at 13A–75A GeV/c
  - (g)  $K^*(892)^0$  production in 0–10% central Ar+Sc collisions at 40A, 75A, and 150A GeV/c
  - (h)  $\Lambda$  production in 0–10% central Ar+Sc collisions at 40A and 150A GeV/c
  - (i)  $h^-$  intermittency in 0–20% central Xe+La collisions at 150A GeV/c



- (j)  $\pi^-$ ,  $K^+$ , and  $K^-$  production in 0–10% central Xe+La collisions at 30A, 40A, and 75A GeV/c
- (k)  $D^0 + \bar{D}^0$  production in 0–20% central Xe+La collisions at 150A GeV/c
- (l) results on invariant mass spectra in Pb+Pb data taken in 2022
- (m)  $\phi$  meson production in 0–10% central Ar+Sc collisions at 40A, 75A, and 150A GeV/c

The recent results recently released or in progress by the NA61/SHINE experiment for long-baseline neutrino oscillation experiments and cosmic-ray experiments include:

- (a) double-differential yields of charged and neutral hadrons from  $p+C$  at 90 GeV/c interactions (submitted in 2024)
  - (b) charged hadrons from  $p+C$  at 60 GeV/c interactions (in progress),
  - (c)  $p+NOvA$  target at 120 GeV/c (in progress)
  - (d)  $p+T2K$  target at 31 GeV/c (in progress)
  - (e) proton and antiproton production measurements in  $p+p$  collisions at 158 GeV/c
  - (f) deuteron production measurements in  $p+p$  collisions at 158 GeV/c
  - (g) two-proton femtoscopy measurements in  $p+p$  collisions at 158 GeV/c
  - (h) fragmentation of cosmic-ray nuclei in the Galaxy
- (V) The requested beam periods in 2025 and 2026 are presented in Section 6. The latter includes two weeks in 2025 and four weeks in 2026 for open charm production in Pb+Pb collisions at 150A GeV/c and one nine days of the oxygen ion beam or the study of the onset of fireball and charge–symmetry violation. For hadron beam NA61/SHINE request four weeks of beam time in 2025 for crucial measurements in high-statistics  $p+p$  interactions at 300 GeV/c. It will allow the measurement of  $p+p$  correlations, deuteron production cross sections, and the first-ever antideuteron production cross section in this energy range. Three additional weeks of proton beam at 120 GeV/c are requested to record production with an alternative LBNF/DUNE prototype target with a different graphite density.

## Acknowledgments

We would like to thank the CERN EP, BE, HSE and EN Departments for the strong support of NA61/SHINE.

This work was supported by the Hungarian Scientific Research Fund (grant NKFIH 138136/137812/138152 and TKP2021-NKTA-64), the Polish Ministry of Science and Higher Education (DIR/WK/-2016/2017/10-1, WUT ID-UB), the National Science Centre Poland (grants 2014/14/E/ST2/00018, 2016/21/D/ST2/01983, 2017/25/N/ST2/02575, 2018/29/N/ST2/02595, 2018/30/A/ST2/00226, 2018/31/G/ST2/03910, 2019/33/B/ST9/03059, 2020/39/O/ST2/00277), the Norwegian Financial Mechanism 2014–2021 (grant 2019/34/H/ST2/00585), the Polish Minister of Education and Science (contract No. 2021/WK/10), the European Union’s Horizon 2020 research and innovation programme under grant agreement No. 871072, the Ministry of Education, Culture, Sports, Science and Technology, Japan, Grant-in-Aid for Scientific Research (grants 18071005, 19034011, 19740162, 20740160 and 20039012,22H04943), the German Research Foundation DFG (grants GA 1480/8-1 and project 426579465), the Bulgarian Ministry of Education and Science within the National Roadmap for Research Infrastructures 2020–2027, contract No. D01-374/18.12.2020, Serbian Ministry of Science, Technological Development and Innovation (grant OI171002), Swiss Nationalfonds Foundation (grant 200020117913/1), ETH Research Grant TH-01 07-3, National Science Foundation grant PHY-2013228 and the Fermi National Accelerator Laboratory (Fermilab), a U.S. Department of Energy, Office of Science, HEP User Facility managed by Fermi Research Alliance, LLC (FRA), acting under Contract No. DE-AC02-07CH11359 and the IN2P3-CNRS (France).

## References

- [1] N. Antoniou *et al.*, [NA61/SHINE Collab.], “Study of Hadron Production in Hadron-Nucleus and Nucleus-Nucleus Collisions at the CERN SPS,” Tech. Rep. CERN-SPSC-2006-034, SPSC-P-330, CERN, Geneva, 2006. <https://cds.cern.ch/record/995681>.
- [2] P. von Doetinchem, [NA61/SHINE Collab.], “Addendum to the NA61/SHINE Proposal: Request for high-statistics p+p measurements in Run 3,” tech. rep., CERN, Geneva, 2024. <https://cds.cern.ch/record/2914265>.
- [3] S. Kowalski, [NA61/SHINE Collab.], “Memorandum requesting use of the allocated test beam for data-taking on  $\pi^+ + C$  and  $\pi^- + C$  interactions at 158 GeV/c,” tech. rep., CERN, Geneva, 2024. <https://cds.cern.ch/record/2907307>.
- [4] J. Spanggaard, “Delay Wire Chambers. A Users Guide”, CERN - SL Division, SL-Note-98-023 (BI), 1998’.
- [5] D. Varga, G. Kiss, G. Hamar, and G. Bencédi *Nucl. Instrum. Meth. A* **698** (2013) 11–18.
- [6] A. László, A. Gera, G. Hamar, B. Pálfi, P. Podlaski, B. Rumberger, and D. Varga *Journal of Instrumentation* **19** (2024) P07024, 2405.01285.
- [7] A. Aduszkiewicz *et al.* *Eur. Phys. J. C* **83** (2023) 471.
- [8] W. Brylinski, “Optimalisation of track reconstruction using vertex detector in the NA61/SHINE experiment,” 2018.
- [9] M. Gazdzicki, M. Gorenstein, and P. Seyboth *Int.J.Mod.Phys. E23* (2014) 1430008, arXiv:1404.3567 [nucl-ex].
- [10] A. Aduszkiewicz *et al.*, [NA61/SHINE Collab.], “Report from the NA61/SHINE experiment at the CERN SPS,” Tech. Rep. CERN-SPSC-2017-038, SPSC-SR-221, CERN, Geneva, 2017. <http://cds.cern.ch/record/2287091>.
- [11] H. Adhikary *et al.*, [NA61/SHINE Collab.] *Eur. Phys. J. C* **84** no. 4, (2024) 416, arXiv:2308.16683 [nucl-ex].
- [12] W. Brylinski, M. Gazdzicki, F. Giacosa, M. Gorenstein, R. Poberezhnyuk, S. Samanta, and H. Stroebele arXiv:2312.07176 [nucl-th].
- [13] H. Adhikary *et al.*, [NA61/SHINE Collab.] arXiv:2312.06572 [nucl-ex].
- [14] H. Adhikary *et al.*, [NA61/SHINE Collab.] *Eur. Phys. J. C* **84** no. 9, (2024) 921, arXiv:2312.13706 [hep-ex].
- [15] M. A. Stephanov, K. Rajagopal, and E. V. Shuryak *Phys.Rev. D60* (1999) 114028, arXiv:hep-ph/9903292 [hep-ph].
- [16] M. Stephanov *Phys. Rev. Lett.* **102** (2009) 032301, arXiv:0809.3450 [hep-ph].
- [17] NA61/SHINE common system-size analysis region <https://edms.cern.ch/document/2487456>.
- [18] L. Adamczyk *et al.*, [STAR Collab.] *Phys. Rev. Lett.* **113** (2014) 092301, arXiv:1402.1558 [nucl-ex].
- [19] H. Adhikary *et al.*, [NA61/SHINE Collab.] *Eur. Phys. J. C* **84** no. 7, (2024) 741, arXiv:2401.03445 [nucl-ex].
- [20] N. G. Antoniou, F. K. Diakonov, A. S. Kapoyannis, and K. S. Kousouris *Phys. Rev. Lett.* **97** (2006) 032002, arXiv:hep-ph/0602051 [hep-ph].
- [21] A. Bialas and M. Gazdzicki *Phys. Lett. B* **252** (1990) 483–486.
- [22] F. Becattini, J. Manninen, and M. Gazdzicki *Phys.Rev. C73* (2006) 044905, arXiv:hep-ph/0511092 [hep-ph].

- [23] H. Adhikary *et al.*, [NA61/SHINE Collab.] *Eur. Phys. J. C* **83** no. 9, (2023) 881, arXiv:2305.07557 [nucl-ex].
- [24] H. Adhikary, [NA61/SHINE Collab.] *EPJ Web Conf.* **274** (2022) 06008, arXiv:2211.10504 [hep-ex].
- [25] N. Abgrall *et al.*, [NA61/SHINE Collab.] *Eur. Phys. J. C* **84** no. 8, (2024) 820, arXiv:2402.17025 [hep-ex].
- [26] B. Porfy, "Symmetric Lévy HBT at NA61/SHINE with Ar+Sc," in *21st Zimányi School Winter Workshop on Heavy Ion Physics*. 2021. <https://indico.cern.ch/event/1097820/contributions/4623124>.
- [27] B. Porfy, "Femtосcopy at NA61/SHINE using symmetric Lévy sources," in *23rd Zimányi School Winter Workshop on Heavy Ion Physics (Zimányi School 2023)*. 2023. <https://indico.cern.ch/event/1352455/contributions/5696658>.
- [28] B. Porfy, [NA61/SHINE Collab.], "Femtосcopy at NA61/SHINE using symmetric Lévy sources in central  $^{40}\text{Ar}+^{45}\text{Sc}$  from 40A GeV/c to 150A GeV/c," in *23rd Zimanyi School Winter Workshop*. 6, 2024. arXiv:2406.02242 [nucl-ex].
- [29] S. Pulawski, "NA61/SHINE at CERN," in *15th Workshop on Critical Point and Onset of Deconfinement (CPOD 2024)*. 2024. <https://conferences.lbl.gov/event/1376/contributions/8763>.
- [30] T. Czopowicz, "Search for critical point in NA61/SHINE," in *15th Workshop on Critical Point and Onset of Deconfinement (CPOD 2024)*. 2024. <https://conferences.lbl.gov/event/1376/contributions/8801>.
- [31] A. Rybicki, "Recent results from NA61/SHINE," in *21st International Conference on Strangeness in Quark Matter (SQM 2024)*. 2024. <https://indico.in2p3.fr/event/29792/contributions/136835>.
- [32] B. Porfy, "Femtосcopy using Lévy-type source at NA61/SHINE," in *42nd International Conference on High Energy Physics (ICHEP 2024)*. 2024. <https://indico.cern.ch/event/1291157/contributions/5878237>.
- [33] B. Porfy, [NA61/SHINE Collab.], "Femtосcopy using Lévy-distributed sources at NA61/SHINE," 10, 2024. arXiv:2410.13975 [nucl-ex].
- [34] B. Porfy, "Energy scan results wit Lévy type femtосcopy at NA61/SHINE," in *17th Workshop on Particle Correlations and Femtосcopy (WPCF 2024)*. 2024. <https://indico.in2p3.fr/event/32030/contributions/144103>.
- [35] T. Csorgo, S. Hegyi, and W. A. Zajc *Eur. Phys. J. C* **36** (2004) 67–78, arXiv:nucl-th/0310042.
- [36] T. Csorgo, S. Hegyi, T. Novak, and W. A. Zajc *AIP Conf. Proc.* **828** no. 1, (2006) 525–532, arXiv:nucl-th/0512060.
- [37] H. Adhikary *et al.*, [NA61/SHINE Collab.] *Eur. Phys. J. C* **83** no. 10, (2023) 919, arXiv:2302.04593 [nucl-ex].
- [38] Y. M. Sinyukov *Nucl. Phys. A* **566** (1994) 589C–592C.
- [39] A. Adare *et al.*, [PHENIX Collab.] *Phys. Rev. C* **97** no. 6, (2018) 064911, arXiv:1709.05649 [nucl-ex].
- [40] B. Kozłowski, " $K^*/K$  ratio and the time between freeze-outs for intermediate-mass Ar+Sc system at the SPS energy range," in *21st International Conference on Strangeness in Quark Matter (SQM 2024)*. 2024. <https://indico.in2p3.fr/event/29792/contributions/137388>.
- [41] B. Kozłowski, " $K^*/K$  ratio and the time between freeze-outs for intermediate-mass Ar+Sc system at the SPS energy range," in *42nd International Conference on High Energy Physics (ICHEP 2024)*. 2024. <https://indico.cern.ch/event/1291157/contributions/5878241>.
- [42] B. Kozłowski, " $K^*/K$  ratio and the time between freeze-outs for intermediate-mass Ar+Sc system at the SPS energy range," in *XIII International Conference on New Frontiers in Physics (ICNFP 2024)*. 2024. <https://indico.cern.ch/event/1307446/contributions/5979992>.
- [43] B. Kozłowski, [NA61/SHINE Collab.], " $K^*/K$  ratio and the time between freeze-outs for intermediate-mass Ar+Sc system at the SPS energy range," 9, 2024. arXiv:2409.20229 [nucl-ex].

- [44] A. Rybicki, [NA61/SHINE Collab.], “Recent results from NA61/SHINE,” 9, 2024. [arXiv:2409.19763 \[nucl-ex\]](#).
- [45] C. Markert, G. Torrieri, and J. Rafelski *AIP Conf. Proc.* **631** no. 1, (2002) 533, [arXiv:hep-ph/0206260](#).
- [46] A. Aduszkiewicz *et al.*, [NA61/SHINE Collab.] *Eur. Phys. J. C* **80** no. 5, (2020) 460, [arXiv:2001.05370 \[nucl-ex\]](#).
- [47] M. Abdallah *et al.*, [STAR Collab.] *Phys. Rev. C* **107** no. 3, (2023) 034907, [arXiv:2210.02909 \[nucl-ex\]](#).
- [48] A. K. Sahoo *Acta Phys. Polon. Supp.* **16** no. 1, (2023) 1–A132, [arXiv:2209.04863 \[hep-ex\]](#).
- [49] S. Acharya *et al.*, [ALICE Collab.] *Phys. Rev. C* **109** no. 1, (2024) 014911, [arXiv:2308.16115 \[nucl-ex\]](#).
- [50] S. K. Das *et al.* *Int. J. Mod. Phys. E* **31** (2022) 12, [arXiv:2208.13440 \[nucl-th\]](#).
- [51] J. Adams *et al.*, [STAR Collab.] *Phys. Rev. C* **71** (2005) 064902, [arXiv:nucl-ex/0412019](#).
- [52] R. L. Workman *et al.*, [Particle Data Group Collab.] *PTEP* **2022** (2022) 083C01.
- [53] S. Acharya *et al.*, [ALICE Collab.] *Phys. Lett. B* **802** (2020) 135225, [arXiv:1910.14419 \[nucl-ex\]](#).
- [54] A. Acharya *et al.*, [NA61/SHINE Collab.] *Eur. Phys. J. C* **82** no. 4, (2022) 322, [arXiv:2112.09506 \[nucl-ex\]](#).
- [55] T. Anticic *et al.*, [NA49 Collab.] *Phys. Rev. C* **84** (2011) 064909, [arXiv:1105.3109 \[nucl-ex\]](#).
- [56] A. Aduszkiewicz *et al.*, [NA61/SHINE Collab.] *Eur. Phys. J. C* **77** no. 10, (2017) 671, [arXiv:1705.02467 \[nucl-ex\]](#).
- [57] C. Alt *et al.*, [NA49 Collab.] *Phys. Rev. Lett.* **94** (2005) 052301, [arXiv:nucl-ex/0406031](#).
- [58] S. V. Afanasiev *et al.*, [NA49 Collab.] *Phys. Rev. C* **66** (2002) 054902, [arXiv:nucl-ex/0205002](#).
- [59] Y. Balkova, “Lambda baryon production in heavy-ion collisions at the NA61/SHINE experiment,” in *21st International Conference on Strangeness in Quark Matter (SQM 2024)*. 2024. <https://indico.in2p3.fr/event/29792/contributions/137362>.
- [60] Y. Balkova, “Lambda baryon production in heavy-ion collisions at the NA61/SHINE experiment,” in *42nd International Conference on High Energy Physics (ICHEP 2024)*. 2024. <https://indico.cern.ch/event/1291157/contributions/5896549>.
- [61] Y. Balkova, “Probing the onset of deconfinement: recent results from the NA61/SHINE experiment,” in *International school of nuclear physics, 44th Course: From quarks and gluons to hadrons and nuclei Erice, Sicily*. 2023. <http://crunch.ikp.physik.tu-darmstadt.de/erice/2023>.
- [62] T. Alber *et al.*, [NA35 Collab.] *Z. Phys. C* **64** (1994) 195–207.
- [63] C. Alt *et al.*, [NA49 Collab.] *Phys. Rev. C* **78** (2008) 034918, [arXiv:0804.3770 \[nucl-ex\]](#).
- [64] A. Aduszkiewicz *et al.*, [NA61/SHINE Collab.] *Eur. Phys. J. C* **76** no. 4, (2016) 198, [arXiv:1510.03720 \[hep-ex\]](#).
- [65] V. Reyna, “Measurements of negatively charged hadron intermittency in central Xe+La at 150A GeV/c by NA61/SHINE at CERN SPS,” in *15th Workshop on Critical Point and Onset of Deconfinement (CPOD 2024)*. 2024. <https://conferences.lbl.gov/event/1376/contributions/8813>.
- [66] V. Reyna, “Search for the critical point via intermittency analysis in NA61/SHINE at CERN,” in *New Trends in High-Energy and Low-x Physics*. 2024. <https://indico.cern.ch/event/1353482/contributions/5989741>.
- [67] O. Panova, “News on identified hadron production in central nucleus-nucleus collisions from NA61/SHINE at CERN SPS,” in *21st International Conference on Strangeness in Quark Matter (SQM 2024)*. 2024. <https://indico.in2p3.fr/event/29792/contributions/137375>.

- [68] O. Panova, “Diagram of high-energy nuclear collisions. New results on Xe+La central collisions from NA61/SHINE at CERN SPS,” in *New Trends in High-Energy and Low-x Physics*. 2024. <https://indico.cern.ch/event/1353482/contributions/5989742>.
- [69] P. Podlaski, “NA61/SHINE Overview,” in *30th International Conference on Ultra-relativistic Nucleus-Nucleus Collisions (Quark Matter 2023)*. 2023. <https://indico.cern.ch/event/1139644/contributions/5343986>.
- [70] O. Panova, “First results on spectra of identified hadrons in central Xe+La collisions from NA61/SHINE at CERN SPS,” in *30th International Conference on Ultra-relativistic Nucleus-Nucleus Collisions (Quark Matter 2023)*. 2023. <https://indico.cern.ch/event/1139644/contributions/5514531>.
- [71] N. Abgrall *et al.*, [NA61/SHINE Collab.] *Eur. Phys. J. C* **74** no. 3, (2014) 2794, [arXiv:1310.2417](https://arxiv.org/abs/1310.2417) [[hep-ex](#)].
- [72] A. Merzlaya, “First  $D^0 + \bar{D}^0$  measurement in heavy-ion collisions at SPS energies with NA61/SHINE,” in *21st International Conference on Strangeness in Quark Matter (SQM 2024)*. 2024. <https://indico.in2p3.fr/event/29792/contributions/137169>.
- [73] A. Merzlaya, “First  $D^0 + \bar{D}^0$  measurement in heavy-ion collisions at SPS energies with NA61/SHINE,” in *12th International Conference on Hard and Electromagnetic Probes of High-Energy Nuclear Collisions (Hard Probes 2024)*. 2024. <https://indico.cern.ch/event/1339555/contributions/6040873>.
- [74] A. Merzlaya, [NA61/SHINE Collab.], “First  $D^0 + \bar{D}^0$  measurement in heavy-ion collisions at SPS energies with NA61/SHINE,” in *21st International Conference on Strangeness in Quark Matter 2024*. 10, 2024. [arXiv:2410.24014](https://arxiv.org/abs/2410.24014) [[nucl-ex](#)].
- [75] A. Merzlaya “Open charm measurements at the NA61/SHINE experiment at CERN SPS with the new Vertex Detector,” PhD thesis CERN-THESIS-2021-065, Jagiellonian University, 2021. <https://cds.cern.ch/record/2771816>.
- [76] A. Aduszkiewicz *et al.* *Eur. Phys. J. C* **83** no. 6, (2023) 471, [arXiv:2302.00563](https://arxiv.org/abs/2302.00563) [[physics.ins-det](#)].
- [77] L. Rozplochowski, “Energy dependence of  $\phi(1020)$  meson production in nucleus-nucleus collisions at the CERN SPS,” in *21st International Conference on Strangeness in Quark Matter (SQM 2024)*. 2024. <https://indico.in2p3.fr/event/29792/contributions/137136>.
- [78] L. Rozplochowski, [NA61/SHINE Collab.], “Energy dependence of  $\phi(1020)$  meson production in nucleus-nucleus collisions at the CERN SPS,” 10, 2024. [arXiv:2410.02379](https://arxiv.org/abs/2410.02379) [[nucl-ex](#)].
- [79] L. Rozplochowski, “Production of  $\phi(1020)$  mesons in nucleus-nucleus collisions at the CERN SPS,” in *17th Workshop on Particle Correlations and Femtoscopy (WPCF 2024)*. 2024. <https://indico.in2p3.fr/event/32030/contributions/144114>.
- [80] A. Aduszkiewicz *et al.*, [NA61/SHINE Collab.] *Eur. Phys. J. C* **80** no. 3, (2020) 199, [arXiv:1908.04601](https://arxiv.org/abs/1908.04601) [[nucl-ex](#)].
- [81] C. Alt *et al.*, [NA49 Collab.] *Phys. Rev. C* **78** (2008) 044907, [arXiv:0806.1937](https://arxiv.org/abs/0806.1937) [[nucl-ex](#)].
- [82] C. Alt *et al.*, [NA49 Collab.] *Phys. Rev. C* **77** (2008) 024903, [arXiv:0710.0118](https://arxiv.org/abs/0710.0118) [[nucl-ex](#)].
- [83] H. Adhikary *et al.*, [NA61/SHINE Collab.] *Phys. Rev. D* **108** no. 7, (2023) 072013, [arXiv:2306.02961](https://arxiv.org/abs/2306.02961) [[hep-ex](#)].
- [84] H. Adhikary *et al.*, [NA61/SHINE Collab.] *Phys. Rev. D* **107** no. 7, (2023) 072004, [arXiv:2211.00183](https://arxiv.org/abs/2211.00183) [[hep-ex](#)].
- [85] L. Aliaga Soplin, *Neutrino flux prediction for the NuMI beamline*. PhD thesis, William and Mary, 2016.
- [86] K. K. Allison *et al.*, “Numerical results for hadron production from 90 GeV/c proton-carbon interactions.” <https://edms.cern.ch/document/3105275/1>, 2024. CERN-EDMS-3105275.
- [87] H. Adhikary *et al.*, [NA61/SHINE Collab.] [arXiv:2410.23098](https://arxiv.org/abs/2410.23098) [[hep-ex](#)].
- [88] P. von Doetinchem *et al.* *JCAP* **08** (2020) 035, [arXiv:2002.04163](https://arxiv.org/abs/2002.04163) [[astro-ph.HE](#)].

- [89] A. Shukla, A. Datta, P. von Doetinchem, D.-M. Gomez-Coral, and C. Kanitz *Phys. Rev. D* **102** no. 6, (2020) 063004, [arXiv:2006.12707](https://arxiv.org/abs/2006.12707) [astro-ph.HE].
- [90] D.-M. Gomez-Coral, A. Menchaca Rocha, V. Grabski, A. Datta, P. von Doetinchem, and A. Shukla *Physical Review D* **98** no. 2, (2018) 023012, [arXiv:1806.09303](https://arxiv.org/abs/1806.09303) [astro-ph.HE].
- [91] A. Shukla "Light nuclei and antinuclei production in proton-proton interactions," PhD thesis CERN-THESIS-2023-051, University of Hawaii at Manoa, 2023. <https://cds.cern.ch/record/2859334>.
- [92] A. Acharya *et al.*, [NA61/SHINE Collab.], "Report from the NA61/SHINE experiment at the CERN SPS," Tech. Rep. CERN-SPSC-2021-027, SPSC-SR-298, CERN, Geneva, 2021. <https://cds.cern.ch/record/2783036>.
- [93] T. Pierog, I. Karpenko, J. M. Katzy, E. Yatsenko, and K. Werner *Phys. Rev.* **C92** no. 3, (2015) 034906, [arXiv:1306.0121](https://arxiv.org/abs/1306.0121) [hep-ph].
- [94] K. Grebieszko, M. Mackowiak-Pawlowska, and P. Von Doetinchem, [NA61/SHINE Collab.], "Report from the NA61/SHINE experiment at the CERN SPS," tech. rep., CERN, Geneva, 2023. <https://cds.cern.ch/record/2878507>.
- [95] S. Acharya *et al.* *Physics Letters B* **811** (Dec, 2020) 135849. <https://doi.org/10.1016%2Fj.physletb.2020.135849>.
- [96] A. Aduszkiewicz *et al.*, [NA61/SHINE Collab.] *Eur. Phys. J.* **C77** no. 2, (2017) 59, [arXiv:1610.00482](https://arxiv.org/abs/1610.00482) [nucl-ex].
- [97] A. Aduszkiewicz *et al.*, [NA61/SHINE Collab.] [arXiv:2006.02153](https://arxiv.org/abs/2006.02153) [nucl-ex].
- [98] H. Adhikary *et al.*, [NA61/SHINE Collab.] [arXiv:2410.18273](https://arxiv.org/abs/2410.18273) [nucl-ex].
- [99] H. Adhikary *et al.*, [NA61/SHINE Collab.], "Addendum to the NA61/SHINE Proposal: Request for light ions beams in Run 4," Tech. Rep. CERN-SPSC-2023-022, SPSC-P-330-ADD-14, CERN, Geneva, 2023. <https://cds.cern.ch/record/2867952>.
- [100] E. Andronov, M. Kuich, and M. Gaździcki *Universe* **9** no. 2, (2023) 106, [arXiv:2205.06726](https://arxiv.org/abs/2205.06726) [hep-ph].
- [101] A. Acharya *et al.*, [NA61/SHINE Collab.], "Addendum to the NA61/SHINE Proposal: A Low-Energy Beamline at the SPS H2," Tech. Rep. CERN-SPSC-2021-028, SPSC-P-330-ADD-12, CERN, Geneva, 2021. <https://cds.cern.ch/record/2783037>.
- [102] Y. Nagai, [NA61/SHINE Collab.], "Additional Information concerning the Low Energy Beam project," tech. rep., CERN, Geneva, 2022. <https://cds.cern.ch/record/2810696>.
- [103] Y. Nagai, [NA61/SHINE Collab.], "Answer to the request raised in the minutes of the 146th meeting of the SPSC regarding the Low Energy Beam project," tech. rep., CERN, Geneva, 2023. <https://cds.cern.ch/record/2878748>.
- [104] M. Gaździcki, D. Kikola, I. Pidhurskyi, and L. Tinti [arXiv:2305.00212](https://arxiv.org/abs/2305.00212) [hep-ph].